

The Peculiar Chemical Inventory of NGC 2419 – An Extreme Outer Halo “Globular Cluster”¹

Judith G. Cohen², Wenjin Huang³ and Evan N. Kirby^{2,4}

ABSTRACT

NGC 2419 is a massive outer halo Galactic globular cluster whose stars have previously been shown to have somewhat peculiar abundance patterns. We have observed seven luminous giants that are members of NGC 2419 with Keck/HIRES at reasonable SNR. One of these giants is very peculiar, with an extremely low [Mg/Fe] and high [K/Fe] but normal abundances of most other elements. The abundance pattern does not match the nucleosynthetic yields of any supernova model. The other six stars show abundance ratios typical of inner halo Galactic globular clusters, represented here by a sample of giants in the nearby globular cluster M30. Although our measurements show that NGC 2419 is unusual in some respects, its bulk properties do not provide compelling evidence for a difference between inner and outer halo globular clusters.

Subject headings: Galaxy: globular clusters: individual (NGC 2419), Galaxy: formation, Galaxy: halo

1. Introduction

NGC 2419 is a globular cluster (GC) in the outer halo of the Galaxy at a distance of 84 kpc¹. Baumgardt et al. (2009) determined a velocity dispersion for this cluster based

¹Based in part on observations obtained at the W.M. Keck Observatory, which is operated jointly by the California Institute of Technology, the University of California, and the National Aeronautics and Space Administration.

²Palomar Observatory, Mail Stop 249-17, California Institute of Technology, Pasadena, Ca., 91125, jlc(enk)@astro.caltech.edu

³Brion Technologies Inc., 4211 Burton Drive, Santa Clara, Ca. 95054, wenjin.huang@brion.com

⁴Hubble Fellow

¹The distance and other parameters for NGC 2419 are from the 2010 version of the on-line GC database of Harris (1996), based on the photometry of Harris et al. (1997).

on 40 stars which leads to $M/L = 2.05 \pm 0.50 M_{\odot}/L_{\odot}$, a normal value for an old stellar system, with no evidence for dark matter at the present time. Conroy, Loeb, & Spergel (2010) further asserted that this cluster could not have formed in a now-defunct dark matter halo. Harris et al. (1997) obtained a deep CMD of NGC 2419 with HST/WFPC2 and demonstrated that there is no detectable difference in age between it and M92, an ancient, well-studied inner halo GC of comparable metallicity. Furthermore, there is no evidence from CMDs of multiple stellar populations in NGC 2419.

However, some of the characteristics of NGC 2419 are anomalous for a GC. It has the highest luminosity ($M_V \sim -9.6$ mag) of any GC with Galactocentric radius $R > 20$ kpc, higher than all other GCs with $R > 15$ kpc with the exception of M54, which is believed to represent the nuclear region of the Sgr dSph galaxy now being accreted by the Milky Way (Ibata, Gilmore & Irwin 1995; Sarajedini & Layden 1995). NGC 2419 also has an unusually large half-light radius ($r_h = 19$ pc) and core radius ($r_c = 7$ pc) for a massive Galactic GC and a relaxation time which exceeds the Hubble time, also unusual for a GC. Every other luminous GC in the outer halo is considerably more compact. The 2010 version of the on-line database of Harris (1996) lists only three Galactic GCs that lie anomalously above the bulk of the Galactic GCs in the plane r_h vs M_V , one of which is NGC 2419. The other two are M54 and ω Cen, the most luminous Galactic GC, and one with a large internal spread in metallicity, also believed to be the stripped core of a dwarf galaxy accreted by the Milky Way. For these reasons, van den Bergh & Mackey (2004) and Mackey & van den Bergh (2005), among others, suggested that NGC 2419 is also the remnant of an accreted dwarf galaxy. In fact, Irwin (1999) and Newberg et al. (2003) suggested that NGC 2419 is one of many GCs associated with the disrupted Sgr dSph, but Law & Majewski (2010) firmly concluded that it is not. Therefore, the cluster is potentially a piece of an unidentified, tidally disrupted dSph.

To follow up on these earlier suggestions, Cohen et al. (2010) obtained moderate resolution spectra of a large sample of luminous giants in NGC 2419 and analyzed line strengths in the region of the near-infrared Ca triplet. We found that there is a small but measurable spread in Ca abundance of ~ 0.3 dex within this massive metal-poor globular cluster. We present here an analysis of high dispersion spectra of seven luminous giant members of NGC 2419, whose chemical inventory we compare to that inferred from a similar sized sample of luminous RGB members of the nearby inner halo globular cluster M30 (NGC 7099), observed and analyzed in the same way as the NGC 2419 stars. Note that these two globular clusters have the same metallicity in the 2003 version of the on-line database of Harris (1996). We explore two issues:

1. Is the chemical inventory in such a distant cluster identical to that of a globular cluster

of similar [Fe/H] in the inner halo?

2. What star-to-star variations are revealed by our high-dispersion spectra?

2. Observations and Analysis

We obtained high-spectral-resolution and reasonably high-SNR spectra of 7 luminous giants in NGC 2419 using HIRESr (Vogt et al. 1994) on the Keck I 10 m Telescope. The stars were selected from both the early spectroscopic study of Suntzeff, Kraft & Kinman (1988) and the current version of the on-line photometric database described by Stetson (2005). The sample stars range in V from 17.2 to 17.6 mag. The spectral range is 3900 to 8350 Å with gaps between the reddest echelle orders. We used a 1.1 arcsec slit, equivalent to 6.3 pixels at $15\mu/\text{pixel}$, to achieve a spectral resolution of 34,000. The maximum total exposure time for one star was 2.5 hours, split into shorter segments to improve cosmic ray removal. The code MAKEE² was used to reduce the HIRES spectra, which were obtained in various runs over the past 5 years. The majority of the seven spectra have a SNR exceeding 90 per spectral resolution element at 5500 Å in the continuum. The SNR degrades towards the blue, and we often eliminated lines bluer than 5000 Å for species with many detected features. The radial velocities for these seven stars have a mean of -20.6 km/sec with σ of 3.7 km/sec . Cohen et al. (2010) discussed membership issues for NGC 2419 in detail. Our sample of 5 RGB members in the sparse nearby GC M30 (NGC 7099) were observed with the same HIRES configuration; all the resulting spectra are of high SNR. Table 1 gives details of the samples and spectra. Figs. 1 and 2 show CMDs for the full Stetson on-line database (Stetson 2005) as well as our HIRES sample for each of these two GCs with 12 Gyr isochrones from the Y2 grid (Yi et al. 2003) superposed.

The determination of stellar parameters followed our earlier papers, (see, e.g. Cohen & Melendez 2005, and references therein) and is based on $V - I$, $V - J$, and $V - K_s$ where the optical colors are from Stetson (2005) and the infrared colors are from 2MASS (Skrutskie et al. 2006; Cutri et al. 2003). The uncertainties in 2MASS K_s are rather large for the faint NGC 2419 giants, and only two of the NGC 7099 giants have an I mag in the Stetson (2005) database. We use the predicted color grid as a function of T_{eff} , $\log(g)$, and [Fe/H]³

²MAKEE was developed by T.A. Barlow specifically for reduction of Keck HIRES data. It is freely available on the world wide web at the Keck Observatory home page, http://www2.keck.hawaii.edu/inst/hires/data_reduction.html.

³The standard nomenclature is adopted; the abundance of element X is given by $\epsilon(X) = N(X)/N(H)$ on a scale where $N(H) = 10^{12}$ H atoms. Then $[\text{X}/\text{H}] = \log[N(\text{X})/N(\text{H})] - \log[N(\text{X})/N(\text{H})]_{\odot}$, and similarly

from Houdashelt, Bell & Sweigart (2000). If we use the recent T_{eff} – color relations of Casagrande et al (2010), which are not calibrated for such luminous giants, we obtain $T_{\text{eff}} \sim 35$ K lower for the cooler luminosity stars in our sample for NGC 2419, ranging up to 105 K lower for the most luminous star in this GC. The surface gravities were calculated assuming a mass of $0.8 M_{\odot}$, the known distance, and the (low) interstellar extinction to each GC. The isochrone of the upper RGB for a very metal-poor old stellar system is such that an error of 100 K in T_{eff} produces an error of 0.2 dex in the inferred surface gravity using this procedure.

The red giants in our sample in NGC 2419 span 0.36 mag in V and a range of less than 200 K in T_{eff} . The RGB stars in our sample for NGC 7099 are somewhat hotter in the mean due both to the somewhat lower metallicity of this GC and to the scarcity of upper RGB stars in this rather sparse cluster.

The detailed abundance analysis for each of the cluster giants follows J. Cohen’s previous work (see, e.g., Cohen & Melendez 2005) using Kurucz (1993) LTE plane-parallel model stellar atmospheres and the analysis code MOOG (Sneden 1973). The adopted transition probabilities are largely from NIST version 3. Note that the gf values adopted here for the observed Mg I and Ca I lines have been updated from those we consistently used up to the present (see, e.g. Cohen & Melendez 2005) to match the current on-line values in the NIST version 4.0 (Ralchenko et al 2010) database. The changes in abundance resulting from these updates are small, about -0.05 dex for Mg for a typical set of observed lines, and $+0.03$ dex for Ca I where more lines are usually observed, only some of which have gf values that have been updated.

Hyper-fine energy level splitting was used where appropriate, with many such patterns taken from Prochaska et al (2000). The adopted damping constants are those described in Cohen & Melendez (2005).

Although it appears that small non-LTE corrections should be applied for several species, for example Na I (Takeda et al 2003) and Ba II (Mashonkina, Gehren & Bikmaev 2000), for consistency with our earlier work, the only non-LTE correction we have implemented is a fixed value of $+0.60$ dex for the resonance Al I doublet at 3944 and 3961 Å following Baumuller & Gehren (1996), (see also Andrievsky et al 2008). Non-LTE for K I is discussed in §7.

Equivalent widths were measured in some cases by the script described in §3 of Cohen & Melendez (2005), which automatically searches for absorption features, fits a Gaussian, then matches those found to a master line list given the radial velocity of the star. For other sample stars,

for [X/Fe].

W. Huang used an IDL script to determine W_λ for the set of lines in the master list. There was extensive hand checking of weak features, of most rare earth lines, and of many of the strongest accepted lines. Lines with $W_\lambda > 175 \text{ m}\text{\AA}$ were rejected unless the species had only a few detected features. The resulting values, together with the atomic parameters for each line used, are given in Tables 3 and 4.

The W_λ for the 3961 Å Al I line, when given, are particularly uncertain for the NGC 2419 giants; the 3944 Å line was never used due to contamination by CH. Both lines are uncomfortably far in the blue, where the SNR of the HIRES spectra for such faint stars is degraded, but the 3961 Å line is a key feature for this element as the 6690 Å Al I doublet is very weak and difficult to detect at the low metallicity of this GC.

Because of the uncertainty of the photometry for the NGC 2419 giants, we felt free to make small adjustments to the photometrically derived stellar parameters, primarily changing T_{eff} . These adjustments, detailed in Table 2, improved the excitation equilibrium for Fe I lines and the ionization balance between neutral and singly ionized lines of Fe and Ti. No such adjustment exceeded 100 K, and was less than 50 K for four of the NGC 2419 giants. In the case of M30, only one star had T_{eff} modified by more than 20 K. For each star in NGC 2419, we measured 67 to 108 Fe I lines, which allowed us to determine the microturbulent velocity directly from the spectra; every star in our sample in NGC 7099 had 99 or more detected Fe I lines.

Table 5 gives the slope of a linear fit to the Fe abundance deduced from each of the Fe I lines detected in a specific sample star as a function of excitation potential, reduced equivalent width (W_λ/λ), and λ , where the first is most sensitive to the adopted T_{eff} , the second to v_t , and the third indicates any systematic problems in continuum opacity as a function of wavelength. Values are given for both GCs. In the ideal case, these slopes are zero. For NGC 2419 the typical range in χ for the Fe I lines is 0.9 to 4.2 eV; the stars with the best spectra span a larger range from 0.0 to 4.8 eV. The wavelength range for Fe I lines in most of the NGC 2419 (NGC 7099) spectra is $\sim 2400 \text{ \AA}$ ($\sim 3000 \text{ \AA}$), and a typical range in reduced equivalent width for such spectra is -5.4 to -4.5 dex for NGC 2419 and -6.3 to -4.4 dex for NGC 7099. The crucial slope with χ ranged from -0.083 to -0.038 dex/eV for the NGC 2419 sample, and is -0.048 ± 0.007 dex/eV for the M30 RGB sample.

The resulting abundances for the 7 RGB stars in NGC 2419 and the 5 in M30 are given in Tables 6 and 7, where all abundances are relative to Fe I. The adopted Solar absolute abundances for each element can be inferred from the entries in Table 7. With regard to the ionization equilibrium, that for Fe I vs Fe II is generally quite good, within 0.1 dex, for all stars in both NGC 2419 and in M30. The ionization equilibrium of Ti I vs Ti II is somewhat worse, typically within ~ 0.2 dex, with the Ti II lines giving a somewhat higher

Ti abundance.

Tables 8a and 8b give the sensitivity of the derived absolute abundances [X/H] and those relative to Fe [X/Fe] for small variations in the various relevant stellar and analysis parameters.

3. Alternative Choices of Stellar Parameters

The choice of stellar parameters is crucial for determining absolute stellar abundances, although less critical for abundance ratios [X/Fe] as many of the systematic effects cancel, as is shown by comparing the entries for each species in Table 8a with those in Table 8b. We have therefore explored several methods of determining T_{eff} . We call the T_{eff} determined by the mean of that inferred from each available color ($V - I$, $V - J$, and $V - K_s$), the photometric T_{eff} . The value of T_{eff} adopted for the abundance analysis, $T_{\text{eff}}(\text{adopt})$, is initially set to $T_{\text{eff}}(\text{phot})$, with small adjustments permitted to improve the Fe I slopes and the ionization equilibrium as described above.

Another T_{eff} can be determined by assuming that all the stars are RGB members of their cluster, and that all the cluster stars have the same initial chemical inventory and age. Hence they must lie along a single old very metal-poor isochrone. Here we are using a single magnitude, chosen on the basis of its high measurement accuracy and discrimination along the isochrone, to determine $T_{\text{eff}}(\text{iso})$. This removes the issue of random errors in colors, which is of particular concern for NGC 2419, with its large distance and hence faint RGB stars near the limit for 2MASS photometry. With a large enough sample, the “isochrone” itself can be defined from the mean locus of the stars in the cluster CMD, as was done in Cohen & Melendez (2005), see also the large VLT study of Carretta et al. (2010) and references therein. In the present case, even if the HIRES sample in NGC 2419 were much larger, the concern that this particular GC may not be chemically uniform would limit the applicability of such an approach. If the isochrone chosen is appropriate for the cluster, then the mean $\Delta[T_{\text{eff}}(\text{phot}) - T_{\text{eff}}(\text{iso})]$ will be zero. If the isochrone is close, but not exactly that of the cluster, then the mean difference will be a constant.

Table 2 gives the values of the adopted, photometric, and isochrone T_{eff} for the sample of RGB stars in NGC 2419. The rms σ about the mean for the set of available colors from the three we consider is given for the $T_{\text{eff}}(\text{phot})$ in parentheses. The photometric T_{eff} was adopted for the detailed abundance analysis for 3 of the 5 stars in NGC 7099. For the other two, the differences are 18 K (0.8 σ) for S31 and 79 K (1.2 σ) for S34. The isochrone and photometric values of T_{eff} for this nearby GC are essentially identical. For NGC 2419 that

is not the case. The brightest star (S223) at the RGB tip is somewhat redder than would be expected from the isochrone.

4. Inner vs Outer Halo

A comparison of the mean abundance ratios in the two globular clusters discussed here M30 (NGC 7099), at a distance of only 8 kpc, with the very distant outer halo globular cluster NGC 2419 is given in Table 9 and illustrated in detail in Fig. 4. There is no substantive difference between the elemental abundance ratios for luminous red giants in the outer halo cluster NGC 2419 and the ratios of inner halo clusters. The inner halo abundance pattern is also observed in other distant clusters: NGC 7492 ($R_G \sim 25$ kpc, Cohen & Melendez 2005), the low luminosity GC Pal 3 ($R_G \sim 90$ kpc, Koch, Côté & McWilliam 2010), and in coadditions of high-resolution, low-SNR spectra of 19 luminous giants in the very distant, low-luminosity GC Pal 4 ($R_G \sim 109$ kpc, Koch & Côté 2010). The low [C/Fe] ratios seen among the NGC 2419 and M30 luminous giants are common among such stars in inner halo GCs (see, e.g. Briley, Cohen & Stetson 2002), presumably due to depletion via deep mixing.

When comparing Galactic GC abundances to those of dSph satellites of the Galaxy, it has become apparent via extensive surveys in recent years (Cohen & Huang 2009, 2010) and at moderate resolution the extensive work of Kirby et al. (2010) that the metal-poor end of all known systems seems to have, at least to first order, an identical chemical inventory. That should not be a surprise, since differences produced through different star formation rates or gas flow history (accretion and/or outflows) between the dSph satellites and the Galactic GCs will only show up at late times. Initially only the metals produced in and ejected by SNII enrich the system’s gas, and hence, except for small metallicity dependent effects on nucleosynthetic yields, all very metal-poor stellar systems should have identical abundance ratios. Those GCs with peculiar abundance ratios, including no enhancement of the α -elements, have intermediate [Fe/H] and most are known to be associated with the ongoing accretion of the Sgr dSph; examples include Pal 12 (Cohen 2004) with [Fe/H] ~ -0.7 dex, Terzan 7 (Sbordone et al 2005) with [Fe/H] -0.6 dex, as well as Rup 106 (Brown, Wallerstein & Zucker 1997) with [Fe/H] -1.45 dex, whose age is several Gyr less than the bulk of the halo, suggesting an accretion origin.

5. Comparison with Previously Published Abundance Analyses

The only previously published high-dispersion analysis of any star in NGC 2419 is for the star S1305, which was observed by Shetrone, Côté & Sargent (2001)⁴. Our measurement of [Fe/H] is 0.13 dex higher than the value they obtained, which we ascribe largely to our adopted T_{eff} being 125 K higher than theirs. The two sets of [X/Fe] for all elements in common through atomic number 30 (Zn) are in good agreement except for Na. Na is a difficult case as the NaD lines are somewhat corrupted by interstellar features at the cluster's v_r , while the 5682, 5688 Å doublet used by Shetrone, Côté & Sargent (2001) is very weak. Among the heavier elements detected in both studies, only Y (in the form of Y II) has a large discrepancy. There are 3 detected lines from our spectra, and a claim of 4 from theirs, but the line at 4900.1 Å is quite crowded, and perhaps should be ignored. For the two Y II lines in common, our W_{λ} are \sim 20% smaller. Considering how faint this star is ($V = 17.61$ mag) we regard the overall agreement in abundances between the two analyses to be very good.

Shetrone et al. (2003) observed one star in NGC 7099. Once the difference in adopted solar Fe abundance is taken into account, their derived [Fe/H] for this star differs from the mean for our sample of five stars by only 0.05 dex. The abundance ratios agree satisfactorily in most cases, with 7 elements differing in [X/Fe] by less than 0.10 dex. Their UVES observations cover only 4800 to 6800 Å, and so are missing many key blue lines for the rare earths, where the differences in relative abundances between the two studies tend to be the largest. The choice of adopted transition probabilities, particularly for the rare earths, also contributes; we adopted them from the recent studies of Lawler and collaborators, (see, e.g. Lawler et al 2001, for Eu as an example) when available, while Shetrone et al. (2003) tended to use older values.

The Padua group (see, e.g. Carretta et al 2009abc and Carretta et al 2010) has completed a large VLT study of the Na/O anti-correlation in GCs. Although their survey does not include NGC 2419, they have observed a sample of 10 RGB stars in M30 with UVES. Thus far they have published abundances for only the light elements. Table 10 presents a comparison of our results from HIRES at Keck with their UVES/VLT study and highlights the good agreement between these two completely independent detailed abundance analyses for RGB stars in M30.

⁴Shetrone, Côté & Sargent (2001) call this star RH 10. The coordinates of this star, privately communicated from M. Shetrone, match those of S1305.

6. Consistency with Our Previous Deimos Range in Ca Abundance

Our previous medium-resolution study of RGB stars in NGC 2419 (Cohen et al. 2010) uncovered a range in [Ca/H] of a factor of two or three among the sample of 43 stars found to be definite members of this GC. The range in V of these stars is from 17.4 to 19.3 mag. Fig. 5 shows a histogram of [Ca/H] for these stars, on which is superposed the distribution of the giants in NGC 2419 with high quality HIRES spectra analyzed here. The two additional probable members discussed in Cohen et al. (2010), each of which has some remaining concern about membership, are indicated in this figure with cross hatching.

The first point to note is that the histogram of [Ca/H] for an unbiased sample of members of NGC 2419, the moderate resolution Deimos survey of Cohen et al. (2010), is sharply peaked at [Ca/H] -1.95 dex. While there is a rapidly declining tail extending towards higher metallicities, the low metallicity peak dominates, and the fraction of stars in the extended tail is small. The minimum [Ca/H] is -2.0 dex. Only 13 (30%) of the 43 definite members lie outside the range -2.0 to -1.85 dex.

Our sample of RGB stars in NGC 2419 with HIRES spectra good enough for a detailed abundance analysis contains only 7 stars. This sample was, to a large extent, selected by brightness before the full analysis of the moderate resolution spectra was completed. One of these 7 stars (S1131) has [Ca/H] -1.72 dex from its HIRES spectrum (-1.76 dex from its Deimos Ca triplet region analysis) and a second star (S973) is marginally above the -1.85 dex [Ca/H] cutoff at -1.81 dex from our detailed abundance analysis (-1.93 dex from its moderate resolution Deimos spectrum). The others all are more metal-poor than [Ca/H] = -1.85 dex as deduced from both their HIRES and Deimos spectra.

The total range in Ca and Fe abundance within the NGC 2419 sample is small (see Table 6. We used the three different choices of T_{eff} discussed in §2 and given in Table 2 as an indication of the maximum range in this parameter that might be appropriate for each of the NGC 2419 stars⁵. In effect, we carried out the abundance analysis three times for each star using different sets of adopted stellar parameters. We find that for each of these three choices, S1131 *always* has the highest value of [Ca/H] of the 7 stars in the HIRES sample for NGC 2419, and it is ~ 0.2 dex (2 to 3 σ) higher than the mean value for the other 6 stars in this cluster. The Fe abundance for S1131, as derived from either Fe I or Fe II, is always the highest or second highest as well, but is within 1 σ of the mean of the other cluster stars.

The uncertainties in absolute abundances (see Table 8a) are daunting for such a small range in Ca abundance in such a distant cluster with spectra and near-IR photometry that

⁵We adjusted $\log(g)$ appropriately in each case to maintain the star on the RGB.

are less than ideal. Lowering the T_{eff} of S1131 in NGC 2419 by ~ 100 K relative to the other RGB stars in this cluster in our HIRES sample would eliminate its high Ca and Fe abundance. But this requires a change of this one star relative to all the others which is about half of the entire range in T_{eff} spanned by the 7 cluster giants, for which there is no justification. Given the small size of our HIRES sample, all we can say is that the Ca/H distribution of the HIRES sample in NGC 2419 is consistent with that of the Deimos sample, which does appear to show a small but measurable range in Ca/H among the cluster members (Cohen et al. 2010).

Both of two probable additional members of NGC 2419 discussed in Cohen et al. (2010) from the Deimos sample, shown by cross hatching in Fig. 5, have been observed with HIRES. However observations were terminated after the first 30 min exposure revealed concerns about cluster membership. Hence the resulting HIRES spectra for these two stars are not good enough for a detailed abundance analysis. One of these (S951) has a spectrum which appears to be that of a RGB star in this very metal-poor GC, but with v_r off from the cluster mean by $\sim 15 \text{ km s}^{-1}$. This star has a value from an analysis of the Ca triplet lines in its Deimos spectrum of [Ca/H] of -1.91 dex, consistent with the bulk of the cluster population. The concern with the second star, S1673, is twofold; it lies slightly bluer than the main RGB locus of NGC 2419 in $V - I$ (see Fig. 2) and its HIRES spectrum appears metal-rich. The [Ca/H] inferred from its Deimos spectrum (-1.68 dex) puts this star, if it is a member, firmly in the metal-rich tail of the histogram shown in Fig. 5. See Cohen et al. (2010) for further discussion regarding membership in NGC 2419 of these two stars.

There are 13 stars in the Deimos sample that may be members of NGC 2419 with $V < 17.7$, which is slightly fainter than the faintest star in the present HIRES sample analyzed here. In addition to all 7 RGB stars in our present HIRES sample, both of the two probable cluster members discussed above are brighter than that cutoff. This leaves 4 stars brighter than $V = 17.7$ mag without HIRES observations at present, 3 of which have [Ca/H] ~ -1.9 dex. Only one is in the high metallicity tail for NGC 2419.

Our present HIRES sample, which was selected primarily on the basis of brightness given the 84 kpc distance to NGC 2419, is not ideal for exploring the star-to-star variation. The small variations of [Ca/H] or [Fe/H] from the 7 stars with high dispersion spectra are only marginally larger than the uncertainties, but are broadly consistent with our Deimos results (Cohen et al. 2010) which found a range in [Ca/H] within NGC 2419. In the future we hope to provide a sample that better probes the metal-rich tail of NGC 2419 as defined by the larger Deimos sample of Cohen et al. (2010).

7. One Star with a Peculiar Abundance Pattern

One star, NGC 2419 S1131, deviates from the archetypal GC abundance pattern. S1131 is a definite member of NGC 2419 based on its HIRES radial velocity (its heliocentric v_r is -17.2 km s^{-1}) and spectrum; see also Cohen et al. (2010). As discussed above in §6 our detailed abundance analysis suggests that this star is slightly more metal-rich than the other NGC 2419 giants in Fe and Ca as well as several other elements with many detected lines. It has an enhancement of ~ 0.2 dex in [Ca/H] (with slight variation depending on the choice of T_{eff} discussed in §3), corresponding to Ca enhanced by a factor of 1.6, compared to the mean of the other 6 NGC 2419 giants.

It is interesting to note that S1131 is the only one of the six NGC 2419 sample giants included in the moderate resolution study of Cohen et al. (2010) found to be Ca-rich. The remaining 6 NGC 2419 giants in the HIRES sample all lie at the low Ca abundance end of the distribution inferred by Cohen et al. (2010). However, given the small abundance range involved, observations of additional giants believed to be more metal-rich than the bulk of the cluster stars are required for a definitive confirmation for star-to-star variation of Ca, Fe, and other heavy elements within NGC 2419.

Furthermore, NGC 2419 S1131 has some anomalous abundance ratios, irrespective of whether its T_{eff} has been overestimated. It has $[\text{Mg}/\text{Fe}] = -0.47$ dex from five Mg I lines, in contrast to the mean of the other six stars, $+0.44 \pm 0.06$ dex. In deriving the Mg abundance for S1131, the upper limit to the strength of the 5711 Å line was considered as a detection, and the two unblended Mg triplet lines were retained. These two lines give Mg abundances slightly higher than the mean, but the highest Mg abundance is from the 5711 Å line, 0.18 dex above the mean of the 5 lines used. Note that the first ionization potential of Mg is only 0.25 eV lower than that of Fe. The $[\text{Mg}/\text{Fe}]$ measurement would increase by only 0.08 dex if T_{eff} were reduced by 100 K (see Table 8b). The regions of the spectra of two Mg I lines in this star and in S1209, also known as Suntzeff 16 (Suntzeff, Kraft & Kinman 1988), with T_{eff} lower than that of S1131 by only 85 K, are shown in Fig. 3. Although most GCs show a small spread in $[\text{Mg}/\text{Fe}]$ (Gratton, Sneden & Carretta 2004), generally interpreted as the result of proton-burning of Mg into Al in intermediate mass AGB stars, the expected enhancement of Al does not appear to be present in S1131. The abundance pattern of this specific star cannot be reproduced by proton-burning. Furthermore -0.47 dex is an unprecedentedly low $[\text{Mg}/\text{Fe}]$ abundance for a globular cluster star; the only stars that have such low $[\text{Mg}/\text{Fe}]$ ratios are the halo star CS22966-043 (Ivans et al. 2003), a hot SX Phe variable, and stars in dSph satellite galaxies, such as COS 171 in Ursa Minor (Cohen & Huang 2010) and S58 in Sextans (Shetrone, Côté & Sargent 2001). NGC 2419 S1131 is unique in that no other elements appear depleted, including Si. A very low value of Mg and super-solar values of

other alpha elements are inconsistent with any Type II SN yields (e.g., Woosley & Weaver 1995; Nomoto et al. 2006; Heger & Woosley 2010).

In addition, NGC 2419 S1131 also has an unusually high [K/Fe] of +1.13 dex, also illustrated in Fig. 3. This figure includes the spectrum of a rapidly rotating B star to demonstrate that any telluric absorption at the wavelength of the K I line, taking into account the v_r of this GC, is negligible. Furthermore, two other NGC 2419 sample stars were observed on the same run (see Table 1) and do not show this abnormality. This abundance ratio would decrease by less than 0.10 dex if T_{eff} were reduced by 200 K. This is an internal comparison within our NGC 2419 sample, which has a total range in T_{eff} of less than 200 K. Studies of non-LTE corrections for the 7699 Å resonance line of K I (the only line used here) by Andrievsky et al (2010) and by Takeda et al (2010) suggest that the appropriate non-LTE corrections change by only 0.15 dex over such a small range in T_{eff} , ranging from about -0.35 to -0.2 dex. Thus differential non-LTE corrections for K I within our HIRES sample of luminous RGB stars are much too small to explain the deviant potassium abundance of S1131.

Takeda et al (2010) very recently found a red giant in M13 and another in M4 with similarly high [K/Fe]. They ascribe the unexpectedly strong K I resonance lines to an increase in activity or turbulent velocity fields high in the stellar atmosphere where the core of such a strong line is formed. However, while S1131 does show emission on both the red and blue wings of H α , the emission wings of H α in the spectrum of NGC 2419 S223 are considerably stronger, yet this star does not show an anomalously strong K I line. Furthermore if this explanation is correct, other strong resonance lines arising from neutral species of elements with (low) first ionization potentials comparable to that of K should be similarly affected. Unfortunately the NaD lines, the most likely candidates to check, are badly corrupted by interstellar absorption due to the radial velocity of NGC 2419.

A careful inspection of Fig. 3 strongly suggests, by comparison with the spectrum of NGC 2419 S1209, which has a V magnitude only 0.2 mag brighter than S1131, that S1131 is indeed slightly more metal-rich in other species as well as K.

The Li I blend at 6707 Å was too weak to be detected in any of the NGC 2419 stars. The upper limit for the equivalent width of this feature of 7 mÅ in S1131 corresponds to $\log[\epsilon(\text{Li})]$ of -0.01 dex, indicates extensive depletion from the Li production in the Big Bang, typical of red giants, which have extensive surface convection zones.

The stellar parameters, spectra, and analyses have been carefully checked and these specific differences in abundance ratios discussed here (i.e. for Mg and for K) within the NGC 2419 sample are real.

8. Summary

Our key result from the analysis of 7 luminous giant members of the distant outer halo globular cluster NGC 2419 is that one of these stars is extremely peculiar, having a very low [Mg/Fe] ratio, but being normal in all other element ratios except for a high [K/Fe]. Similarly low [Mg/Fe] ratios are seen in stars in dSph satellites of the Galaxy, specifically in Ursa Minor (Cohen & Huang 2010) and in Sextans (Shetrone, Côté & Sargent 2001). But in both cases these stars have low values of other α elements, which is not the case for NGC 2419 S1131. J. Cohen has examined and analyzed spectra of $\gtrsim 100$ stars in Galactic GCs, and has never seen one similar to S1131 in NGC 2419.

Furthermore, the HIRES spectra support the small range in metallicity within the giants in NGC 2419 found by Cohen et al. (2010), which might suggest that this distant outer halo GC is the remnant of an accreted dwarf galaxy. A definitive result will require further observations of the faint upper RGB stars in this GC, concentrating on those whose moderate resolution Deimos spectra from Cohen et al. (2010) suggest they are more metal-rich than the bulk of the stars in this cluster, which will be carried out in a future campaign.

Ignoring the limited peculiarities of S1131, we find that there is no substantive difference between the mean behavior of the abundance ratios for six other red giants in NGC 2419 and those ratios characteristic of the inner halo despite the structural peculiarities of NGC 2419. The influence of star formation rates and other aspects of the detailed chemical evolution of a stellar system only affect such ratios once star formation has been underway long enough for sources other than SNII to become important contributors, which does not seem to be the case in very metal-poor systems such as NGC 2419, nor in the most metal-poor stars in the dSph satellites of the Milky Way (Cohen & Huang 2009, 2010; Kirby et al 2011).

Thus, like the previous studies based on detailed abundance analyses of individual or co-added stellar spectra of stars in distant outer halo clusters, the chemical inventory of the globular cluster system appears to be independent of location. With the exception of those clusters known to be associated with the currently disrupting Sgr dSph galaxy, every globular cluster exhibits the same trends as a function of overall cluster metallicity—parameterized by [Fe/H]—irrespective of kinematics or location within the halo.

The existence of a metallicity gradient in the Galactic halo is controversial. Carollo et al. (2007) found evidence for a break in the metallicity distribution of halo field stars in the sense that the more distant stars are more metal-poor; this conclusion is supported by de Yong et al (2010). Furthermore, Carollo et al. (2007) showed that the metallicity within the outer halo population displays a gradient toward even lower metallicities for the most distant stars or stars showing the highest magnitude of rotation retrograde to the Milky

Way disk. However, both Sesar et al. (2011) and Schoenrich et al. (2010) improved upon Carollo et al.’s study. These new works, which are disputed by Beers et al. (2011), found no evidence for a dichotomous halo, particularly in regard to the kinematics and density profile. Our measurements for NGC 2419 additionally provide evidence against a dichotomy in detailed abundances. The outer halo globular clusters show the same bulk abundance properties—and, by extension, (short) star formation timescales—as the inner halo globular clusters.

We are grateful to the many people who have worked to make the Keck Telescope and its instruments a reality and to operate and maintain the Keck Observatory. The authors wish to extend special thanks to those of Hawaiian ancestry on whose sacred mountain we are privileged to be guests. Without their generous hospitality, none of the observations presented herein would have been possible. We thank Alex Heger and Ken Nomoto for helpful conversations. J.G.C. and W.H. thank NSF grants AST-0507219 and AST-0908139 for partial support. Work by E.N.K. was supported by NASA through Hubble Fellowship grant HST-HF-01233.01 awarded to ENK by the Space Telescope Science institute, which is operated by the Association of Universities for Research in Astronomy, Inc., for NASA, under contract NAS 5-26555.

REFERENCES

- Alcaino, G. & Liller, W., 1980, AJ, 85, 1330
- Andrievsky, S. M., Spite, M., Korotin, S. A., Spite, F. & Bonifacio, P., 2008, A&A, 481, 481
- Andrievsky, S. M., Spite, M., Korotin, S. A., Spite, F., Bonifacio, P., Cayrel, R., Francois, P. & Hill, V., A&A, 509, 88
- Baumgardt, H., Côté, P., Rejkuba, M., Mieske, S., Djorgovski, S. G. & Stetson, P., 2009, MNRAS, 396, 2051
- Baumuller D.G. & Gehren, T., 1996, A&A, 307, 961
- Beers, T. C. et al., 2011, ApJ(submitted) (available as arXiv:1104.2513)
- Bolte, M., 1987, ApJ, 319, 760
- Briley, M. M., Cohen, J. G. & Stetson, P. B., 2002, ApJ, 579 L17
- Brown, J.A., Wallerstein, G. & Zucker, D., 1997, AJ, 114, 180
- Carollo, D. et al, 2007, Nature, 450, 1020
- Carretta, E. et al, 2009, A&A, 505, 117
- Carretta, E., Bragaglia, A., Gratton, R., Lucatello, S., 2009, A&A, 505, 139
- Carretta, E., Bragaglia, A., Gratton, R., D’Orazi, V. & Lucatello, S., 2009, A&A, 508, 695
- Carretta, E., Bragaglia, A., Gratton, R., Lucatello, S., Bellazzini, M. & D’Orazi, V., 2010, ApJ, 712, 1
- Casagrande, L., Ramirez, I., Melendez, J. & Bessell, M., 2010, A&A, 512, A54
43, 207
- Cohen, J. G., 2004, AJ, 127, 1545
- Cohen, J. G. & Melendez, J., 2005a, AJ, 129, 303
- Cohen, J. G. & Melendez, J., 2005b, AJ, 129, 1607
- Cohen, J. G. & Huang, W., 2009, ApJ, 701, 1053
- Cohen, J. G. & Huang, W., 2010, ApJ, 719, 931

- Cohen, J. G., Kirby, E. N., Simon, J. & Geha, M., 2010, ApJ, 725, 288
- Conroy, C., Loeb, A., & Spergel, D. 2010, arXiv:1010.5783
- Cutri, R. M. et al, 2003, “Explanatory Supplement to the 2MASS All-Sky Data Release,
<http://www.ipac.caltech.edu/2mass/releases/allsky/doc/expsup.html>
- D’Orazi, V., Gratton, R., Lucatello, S., Carretta, E., Bragaglia, A. & Marino, A. F., 2010,
ApJ, 719, L213
- de Jong, J. T. A., Yanny, B., Rix, H. W., Dolphin, A., Martin, N. F. & Beers, T. C., 2010,
ApJ, 714, 663
- Gratton, R., Sneden, C. & Carretta, E., 2004, ARA&A, 42, 385
- Harris, W. E., 1996, AJ, 112, 1487
- Harris, W. E. et al, 1997 AJ, 114, 1030
- Heger, A. & Woosley, S. E., 2010, ApJ, 724, 341
- Houdashelt, M. L., Bell, R. A. & Sweigart, A. V., 2000, AJ, 119, 1448
- Ibata, R. A., Gilmore, G. F. & Irwin, M. J., 1995, MNRAS, 277, 781
- Irwin, M. 1999, ASP Conf. Ser. 192, The Stellar Content of Local Group Galaxies, ed.
P. Whitelock & R. Cannon (San Francisco: ASP), 409
- Ivans, I. I., Sneden, C., James, C. R., Preston, G. W., Fulbright, J. P., Höflich, P. A., Carney,
B. W., & Wheeler, J. C. 2003, ApJ, 592, 906
- Kirby, E. N., Cohen, J.G., Smith, G. H., Majewski, S. R., Sohn, S. T. & Guhathakurta, P.,
2011, ApJ, 727, 79
- Koch, A. & Côté, P., 2010, A&A, 517, A59
- Koch, A. Côté, P. & McWilliam, A., 2009, A&A, 506, 729
- Kurucz, R. L., 1993, ATLAS9 Stellar Atmosphere Programs and 2 km/s Grid, (Kurucz
CD-ROM No. 13)
- Law, D. R., & Majewski, S. R. 2010, ApJ, 718, 1128
- Lawler, J. E., Wickliffe, M. E., Den Hartog, E. A. & Sneden, C., 2001, ApJ, 563, 1075

- Mackey, A. D. & van den Bergh, S., 2005, MNRAS, 360, 631
- Masonkina, L, Gehren, T. & Bikmaev, I., 2000, A&A, 343, 519
- Newberg, H. J., et al. 2003, ApJ, 596, L191
- Nomoto, K., Tominaga, N., Umeda, H., Kobayashi, C., & Maeda, K. 2006, Nuclear Physics A, 777, 424
- Prochaska, J. X., Naumov, S. O., Carney, B. W., McWilliam, A. & Wolfe, A. M., 2000, AJ, 120, 2513
- Ralchenko, Yu., Kramida, A. E., Reader, J. & the NIST ASD Team, 2010, NIST Atomic Spectra Database (version 4.0), <http://physics.nist.gov/asd>
- Sarajedini, A. & Layden, A. C., 1995, AJ, 109, 1086
- Sbordone, L., Bonifacio, P., Marconi, G., Buonanno, R. & Zaggia, S., 2005, A&A, 437, 905
- Schoenrich, R., Asplund, M., & Casagrande, L. 2010, MNRAS, submitted, arXiv:1012.0842
- Sesar, B., Juric, M., & Ivezić, Z. 2011, ApJ, accepted, arXiv:1011.4487
- Shetrone, M., Côté, P. & Sargent, W. L. W., 2001, ApJ, 568, 592
- Shetrone, M., Venn, K. A., Tolstoy, E., Primas, F., Hill, V. & Kaufer,A., 2003, AJ, 125, 648
- Skrutskie, M. F. et al, 2006, AJ, 131, 1163
- Sneden, C., 1973, Ph.D. thesis, Univ. of Texas
- Stetson, P. B., 2005, PASP, 117, 563
- Suntzeff, N., Kraft, R. P. & Kinman, T. D., 1988, AJ, 95, 91
- Takeda, Y., Zhao, G., Takada-Hidai, M., Chen, Y. Q., Saito, Y. & Zhang, H. W., Chinese Jrl. Astron. Astrophys, 3, 311
- Takeda, Y., Kaneko, H., Matsumoto, N., Oshinio, S., Ito, H. & Shibuya, T., 2010, PASJ, 61, 563
- van den Bergh, S. & Mackey, D., 2004, MNRAS, 354, 713
- Vogt, S. E. et al. 1994, SPIE, 2198, 362
- Woosley, S. E., & Weaver, T. A. 1995, ApJS, 101, 181

Yi, S., Kim, Y.-C., Demarque, P. & Alexander, D. R., 2003, ApJS, 143, 499

Table 1. Data for Red Giant Members of NGC 2419 and of NGC 7099 With HIRES/Keck Spectra

Name ^a	V ^a (mag)	T _{eff} , log(<i>g</i>), <i>v_t</i> ^b (K, dex, km s ⁻¹)	[Fe/H](Fe I) (dex)	Date ^c	Exp. Time (sec)	SNR ^d	<i>v_r</i> (km s ⁻¹)
NGC 2419							
Stet 223 ^e	17.25	4250, 0.50, 2.4	−2.09	2/2010	8400	> 100	−22.4
Stet 810	17.31	4330, 0.60, 2.1	−2.00	11/2010	7200	> 100	−22.6
Stet 973 ^f	17.45	4320, 0.70, 2.1	−1.98	9/2006	3200	39	−21.9
Stet 1131	17.61	4435, 0.75, 2.2	−1.95	2/2010	9000	95	−16.8
Stet 1209 ^g	17.41	4350, 0.40, 2.1	−2.20	11/2010	7200	93	−19.0
Stet 1305 ^h	17.61	4400, 0.80, 2.3	−2.17	9/2008	3000	52	−16.8
Stet 1814 ⁱ	17.27	4370, 0.55, 2.3	−2.04	2/2010	5400	90	−26.1
NGC 7099							
Stet 31	13.92	4790, 1.63, 2.2	−2.39	9/2006	1200	> 100	−185.8
Stet 34	13.57	4658, 1.13, 2.0	−2.32	9/2006	1200	> 100	−188.1
AL 38 ^j	13.27 ^j	4653, 1.10, 2.1	−2.47	9/2006	900	> 100	−185.6
Stet 42	14.70	4935, 2.03, 1.8	−2.46	9/2006	1200	> 100	−190.1
Stet 81 ^l	14.25	5050, 1.70, 2.2	−2.48	9/2006	1200	> 100	−185.9

^aStar IDs and *V* mags are from the online version of the database of Stetson (2005).

^bThese are the values adopted for the abundance analysis.

^cDate of the best spectrum. Earlier low SNR spectra were taken for several of the NGC 2419 stars.

^dSNR per spectral resolution element in the continuum at 5500 Å.

^eStetson 223 = Suntzeff 1.

^fStetson 973 = Suntzeff 15.

^gStetson 1209 = Suntzeff 16.

^hStetson 1305 = RH 10 (private communication from M. Shetrone), previously observed by

Shetrone, Côté & Sargent (2001).

ⁱStetson 1814 = Suntzeff 14.

^jID from Alcaino & Liller (1980).

^k V mag from Bolte (1987).

^lS81 lies slightly bluer in $B - V$ than the mean RGB locus.

Table 2. Choice of T_{eff} For Red Giant Members of NGC 2419

Name ^a	V^{a} (mag)	T_{eff} (Adopt) (K)	$T_{\text{eff}}(\text{Phot}), \sigma(T_{\text{eff}})^{\text{b}}$ (K)	T_{eff} (Isochrone) (K)
NGC 2419				
Stet 223	17.25	4250	4150 (20)	4264
Stet 810	17.31	4330	4372 (20)	4286
Stet 973	17.45	4320	4392 (39)	4340
Stet 1131	17.61	4435	4428 (35) ^c	4384
Stet 1209	17.41	4350	4328 (46)	4327
Stet 1305	17.61	4400	4488 (86) ^d	4385
Stet 1814	17.27	4370	4355 (55)	4274
NGC 7099				
S31	13.92	4790	4770 (24)	...
S34	13.57	4658	4658 (27)	...
AL38	13.27	4655	4655 (52) ^e	...
S42	14.70	4935	4935 (44) ^e	...
S81	14.25	5050	4970 (64) ^e	...

^aStar IDs and V mags are mostly from the online version of the database of Stetson (2005). See notes to Table 1 for details.

^brms of T_{eff} as derived from the available colors including $V - I$, $V - J$, and $V - K_s$.

^cUncertainty in 2MASS K_s is 0.09 mag.

^dUncertainty in 2MASS K_s is 0.10 mag.

^eNo I mag available.

Table 3. Equivalent Widths for NGC 2419 RGB Stars

λ (Å)	Ion	χ_{exc} (eV)	$\log gf$ (dex)	S223 (mÅ)	S1814 (mÅ)	S810 (mÅ)	S1209 (mÅ)	S973 (mÅ)	S1305 (mÅ)	S1131 (mÅ)
6707.8	Li I	0.00	0.178	≤ 7.0
6300.30	[O I]	0.00	-9.780	36.7	54.7
6363.78	[O I]	0.02	-10.300	23.5
5682.63	Na I	2.10	-0.700	30.3	14.9	6.0	13.0
5688.19	Na I	2.10	-0.420	46.0	...	15.0	36.0
5889.95	Na I	0.00	0.110	362.0	376.0	...
5895.92	Na I	0.00	-0.190	236.0	282.0	279.0	355.0	...
4703.00	Mg I	4.34	-0.440	92.0	140.0	96.4	125.0	123.0	102.3	56.0
5172.70	Mg I	2.71	-0.380	340.0	365.0	312.2	224.0
5183.62	Mg I	2.72	-0.160	406.8	419.9	365.6	266.0
5528.40	Mg I	4.34	-0.498	158.5	150.0	138.7	139.2	122.2	120.9	71.0
5711.09	Mg I	4.34	-1.724	44.0	48.0	47.5	43.3	73.0	40.8	≤ 15.5
3961.52	Al I	0.00	-0.340	226.1	228.0	121.5	203.6	240.5
6696.02	Al I	3.14	-1.340	15.7	11.5	7.5	5.0	10.9
4102.94	Si I	1.91	-3.140	150.8
5665.55	Si I	4.92	-2.040	21.5
5690.43	Si I	4.93	-1.870	...	18.0	18.7	...	16.0
5772.15	Si I	5.08	-1.750	13.6
5948.54	Si I	5.08	-1.230	21.8	22.8	15.0	20.3	35.3
6155.13	Si I	5.62	-0.760	24.6
6237.32	Si I	5.62	-1.010	21.1
7003.57	Si I	5.96	-0.830	11.5
7005.89	Si I	5.98	-0.730	21.0	15.5	19.1
7034.90	Si I	5.87	-0.880	15.7
7405.77	Si I	5.61	-0.820	28.8	13.7	39.0
7415.95	Si I	5.61	-0.730	16.0	24.2	25.4	29.0
7423.50	Si I	5.62	-0.580	26.3	26.2	42.0	32.7	44.3
7698.97	K I	0.00	-0.168	151.6	133.0	129.1	114.6	...	108.3	175.0
4454.79	Ca I	1.90	0.260	...	154.0
4578.56	Ca I	2.52	-0.558	41.4
5512.99	Ca I	2.93	-0.300	...	29.8	22.1	...	32.3
5581.96	Ca I	2.52	-0.710	48.6	42.4	...	35.0	50.9	47.2	56.0
5588.75	Ca I	2.52	0.210	111.7	110.0	93.5	98.2	109.7	79.0	120.7
5590.11	Ca I	2.52	-0.710	47.7	43.3	47.2	47.0	57.2	41.2	57.2
5594.46	Ca I	2.52	-0.050	...	83.0	...	85.2	...	94.0	98.3
5601.28	Ca I	2.52	-0.690	53.8	49.7	54.3	42.0	50.3	68.5	67.3
5857.45	Ca I	2.93	0.230	76.6	68.0	72.4	69.2	90.0	62.3	87.2
6161.30	Ca I	2.52	-1.030	24.7	18.7	19.9	19.0	32.4	...	28.5
6162.17	Ca I	1.90	-0.090	...	161.8	150.9	147.0	160.9	145.0	164.7
6166.44	Ca I	2.52	-0.900	25.9	19.3	...	24.2	22.1	18.0	32.8
6169.04	Ca I	2.52	-0.540	58.0	45.7	50.6	39.2	63.0	45.3	47.2
6169.56	Ca I	2.52	-0.270	59.9	63.4	67.4	56.8	64.0	52.0	73.0
6471.66	Ca I	2.52	-0.590	52.8	47.7	52.9	39.7	54.2	53.1	62.0
6493.78	Ca I	2.52	0.140	95.7	92.7	89.9	91.3	111.2	90.4	101.8
6499.65	Ca I	2.54	-0.590	38.2	40.5	47.3	40.0	48.2

Table 3—Continued

λ (Å)	Ion	χ_{exc} (eV)	$\log gf$ (dex)	S223 (mÅ)	S1814 (mÅ)	S810 (mÅ)	S1209 (mÅ)	S973 (mÅ)	S1305 (mÅ)	S1131 (mÅ)
6717.68	Ca I	2.71	-0.610	55.3	54.2	...	44.9	61.2	55.6	62.9
7148.15	Ca I	2.71	0.218	111.3	100.8	130.2	101.8	112.4
4670.41	Sc II	1.36	-0.580	...	89.2
5526.79	Sc II	1.77	0.130	111.0	92.0	86.1	78.4	71.0	80.8	122.0
5657.90	Sc II	1.51	-0.500	99.8	91.5	79.3	80.9	75.7	64.9	120.0
5667.15	Sc II	1.50	-1.240	43.2	36.2	31.7	34.5	34.0	34.2	54.1
5669.04	Sc II	1.50	-1.120	43.7	50.8	35.2	...	40.6	50.8	71.3
5684.20	Sc II	1.51	-1.080	54.7	43.7	49.0	47.2	42.1	29.9	73.1
6245.64	Sc II	1.51	-1.130	55.6	51.1	49.4	41.3	48.4	46.9	73.9
6604.59	Sc II	1.36	-1.310	42.0	35.0	43.5	38.8	55.0	43.1	66.1
4512.74	Ti I	0.84	-0.480	75.4	63.2	...	53.4	77.5
4518.03	Ti I	0.83	-0.230	...	83.5	...	69.0
4533.25	Ti I	0.85	0.480	...	120.6	101.7	107.4	124.0
4534.78	Ti I	0.84	0.280	129.7	107.8	97.8	81.0	106.0
4548.77	Ti I	0.83	-0.350	94.0	75.0	57.9	78.5	75.3
4555.49	Ti I	0.85	-0.490	...	51.9	...	46.7	57.0
4681.92	Ti I	0.05	-1.070	...	110.9	110.5	111.6	100.4
4981.74	Ti I	0.85	0.500	...	135.0	136.6	115.2	133.8
4999.51	Ti I	0.83	0.250	152.8	137.0	111.4	115.1	139.4	107.1	119.2
5022.87	Ti I	0.83	-0.430	99.3	86.3	81.2	77.2	114.0	74.4	76.5
5039.96	Ti I	0.02	-1.130	163.1	132.5	118.7	111.0	108.0	95.8	104.1
5173.75	Ti I	0.00	-1.120	157.6	128.4	120.3	114.3	133.8	112.0	115.1
5210.39	Ti I	0.05	-0.880	...	157.0	142.5	123.3	147.0	143.0	126.3
5426.26	Ti I	0.02	-3.010	30.2
5490.15	Ti I	1.46	-0.933	10.5
5866.45	Ti I	1.07	-0.840	56.9	45.3	51.9	27.6	38.7	32.4	39.9
5922.11	Ti I	1.05	-1.470	31.1	10.7	17.3
5941.75	Ti I	1.05	-1.520	15.8	17.7	15.2
5953.16	Ti I	1.89	-0.329	19.5	19.8	20.6
5965.83	Ti I	1.88	-0.409	18.6	18.0	18.0	13.9
5978.54	Ti I	1.87	-0.496	12.8
6126.22	Ti I	1.07	-1.420	30.0	19.1	...	15.7	...	23.0	25.5
6258.10	Ti I	1.44	-0.355	47.0	41.2	46.2	26.2	...	31.0	39.0
6258.71	Ti I	1.46	-0.240	61.1	41.4	52.1	31.2	42.2	34.4	44.0
6261.10	Ti I	1.43	-0.479	44.4	32.2	32.6	30.6	38.4
6743.12	Ti I	0.90	-1.630	21.5	20.4	16.8	...	15.3
4399.77	Ti II	1.24	-1.290	...	147.5	155.4
4417.72	Ti II	1.16	-1.160	...	150.0	159.5
4501.28	Ti II	1.12	-0.760	149.4	173.4
4563.77	Ti II	1.22	-0.820	134.4	164.1
4571.98	Ti II	1.57	-0.340	161.1	173.7
4583.41	Ti II	1.16	-2.870	49.2	69.1
4589.95	Ti II	1.24	-1.650	134.0	136.2	99.1	116.2	126.8
4657.20	Ti II	1.24	-2.320	78.4	80.7	90.0
4708.67	Ti II	1.24	-2.370	74.3	95.2	...	83.0	58.0	69.0	96.0

Table 3—Continued

λ (Å)	Ion	χ_{exc} (eV)	$\log gf$ (dex)	S223 (mÅ)	S1814 (mÅ)	S810 (mÅ)	S1209 (mÅ)	S973 (mÅ)	S1305 (mÅ)	S1131 (mÅ)
4762.78	Ti II	1.08	-2.710	83.0
4798.54	Ti II	1.08	-2.670	65.4	...
4865.62	Ti II	1.12	-2.810	68.1	75.0	62.0	59.0	74.5
4911.20	Ti II	3.12	-0.340	30.0	...	25.0	48.0	32.0
5185.91	Ti II	1.89	-1.460	104.2	86.0	74.1	76.9	83.0	89.0	86.0
5670.85	V I	1.08	-0.425	22.0
5703.57	V I	1.05	-0.212	17.0	9.8	21.7	17.1
6081.44	V I	1.05	-0.579	10.3
6090.22	V I	1.08	-0.062	24.3	19.6	24.9	20.8	29.9	...	25.5
6199.20	V I	0.29	-1.280	29.9	21.5
6243.10	V I	0.30	-0.978	33.1	35.4	49.1	22.9	49.3	16.9	28.7
6251.82	V I	0.29	-1.340	18.0	12.3	21.0	...	10.6
6274.64	V I	0.27	-1.670	10.7
6285.14	V I	0.28	-1.510	19.1	21.0	...
4545.96	Cr I	0.94	-1.380	86.9	91.0	69.2	58.6	77.1
4600.76	Cr I	1.00	-1.280	...	62.1	...	80.3	75.4
4616.13	Cr I	0.98	-1.210	88.4	80.4	78.4
4626.18	Cr I	0.97	-1.340	92.5	74.1	67.4	57.0	81.8
4652.17	Cr I	1.00	-1.030	98.2	95.2	89.7	79.2
5206.04	Cr I	0.94	0.030	174.0	175.0	139.8	...
5298.28	Cr I	0.98	-1.170	111.2
5409.80	Cr I	1.03	-0.710	169.0	136.3	131.4	111.8	131.8	108.5	132.7
6979.80	Cr I	3.46	-0.411	6.1
4033.06	Mn I	0.00	-0.620	238.4
4754.04	Mn I	2.28	-0.090	74.1	88.7	75.8	83.5	77.8	63.6	80.2
4783.42	Mn I	2.30	0.042	96.6	86.5	91.6	81.4	91.4	79.8	84.1
4823.51	Mn I	2.32	0.140	99.5	96.8	87.3	82.7	118.0	88.0	94.7
5394.69	Mn I	0.00	-3.503	101.0	77.0	88.8	57.9	84.2	...	67.0
6013.50	Mn I	3.07	-0.252	13.5	9.9
6021.80	Mn I	3.08	0.034	36.3	35.2	37.4	27.2	...	28.0	38.9
4489.75	Fe I	0.12	-3.970	146.3
4494.57	Fe I	2.20	-1.140	142.6
4531.16	Fe I	1.49	-2.150	147.8	126.7
4602.95	Fe I	1.49	-2.220	129.3	137.3	148.3
4625.05	Fe I	3.24	-1.348	75.6	48.4	57.8	50.7	73.1
4788.77	Fe I	3.24	-1.806	34.1	29.7	35.9	31.5
4871.33	Fe I	2.86	-0.360	...	134.3	127.9	126.3
4872.14	Fe I	2.88	-0.570	...	127.6	128.7
4891.50	Fe I	2.85	-0.110	...	157.9	149.4	147.3	152.5
4919.00	Fe I	2.86	-0.340	161.9	147.9	137.6	135.0	136.0	...	137.3
4920.51	Fe I	2.83	0.150	188.5
5083.34	Fe I	0.96	-2.960	...	172.5	143.7	150.6	157.1	141.9	150.3
5166.28	Fe I	0.00	-4.200	174.0	179.9	...	167.6	163.1
5171.61	Fe I	1.48	-1.790	157.0	170.6	175.5	...	173.0
5192.35	Fe I	3.00	-0.420	157.0	136.9	122.2	126.3	116.0	109.0	...

Table 3—Continued

λ (Å)	Ion	χ_{exc} (eV)	$\log gf$ (dex)	S223 (mÅ)	S1814 (mÅ)	S810 (mÅ)	S1209 (mÅ)	S973 (mÅ)	S1305 (mÅ)	S1131 (mÅ)
5194.95	Fe I	1.56	-2.090	...	165.9	154.9	159.5	159.4	152.9	150.4
5198.72	Fe I	2.22	-2.140	128.3	112.9	103.4	95.8	97.9	95.2	104.3
5216.28	Fe I	1.61	-2.150	...	165.4	155.4	137.1	...	133.0	142.8
5217.40	Fe I	3.21	-1.070	78.9	74.7	102.0	68.2	77.0
5232.95	Fe I	2.94	-0.100	...	157.3	145.2	141.1	168.6	139.6	159.4
5393.18	Fe I	3.24	-0.720	114.5	108.1	105.2	87.4	131.0	84.1	105.3
5410.92	Fe I	4.47	0.400	71.2	63.2	56.9	62.7	69.6	46.2	60.1
5415.21	Fe I	4.39	0.640	85.7	87.4	84.2	78.3	79.1	73.3	89.0
5424.08	Fe I	4.32	0.510	107.8	97.7	89.9	85.9	82.6	86.0	97.9
5445.05	Fe I	4.39	-0.030	56.6	48.3	...	51.1	...	41.1	65.8
5466.39	Fe I	4.37	-0.620	25.0	12.8	25.5	20.6	28.2
5473.90	Fe I	4.15	-0.690	23.7	...	30.1	24.3	34.5	25.6	27.2
5487.77	Fe I	4.14	-0.620	31.5	34.6	38.8	26.3	59.2	...	39.2
5497.52	Fe I	1.01	-2.830	174.3	164.2	170.3	165.1	...
5501.46	Fe I	0.96	-3.050	161.6	155.1	152.2	147.9	164.8
5506.79	Fe I	0.99	-2.790	167.1	168.1	158.9	...
5522.45	Fe I	4.21	-1.450	7.2
5554.88	Fe I	4.55	-0.350	16.7	26.7	29.6	17.9	20.2
5567.39	Fe I	2.61	-2.670	49.8	36.7	42.2	39.2	...	29.9	44.9
5569.62	Fe I	3.42	-0.486	106.7	94.0	99.4	87.5	92.4	80.0	98.6
5572.84	Fe I	3.40	-0.275	129.1	116.6	116.3	111.2	...	108.8	115.4
5576.09	Fe I	3.43	-0.920	90.1	76.8	82.5	69.9	80.3	74.9	81.8
5586.76	Fe I	3.37	-0.140	143.8	137.5	120.5	120.8	125.3	122.0	131.0
5624.04	Fe I	4.39	-1.220	7.2
5624.54	Fe I	3.42	-0.755	100.4	78.9	86.2	72.4	103.2	68.0	86.9
5641.44	Fe I	4.26	-1.080	...	21.6	22.3
5662.52	Fe I	4.18	-0.570	...	25.2	37.4	41.4	...	29.7	35.7
5679.02	Fe I	4.65	-0.820	...	9.6
5701.54	Fe I	2.56	-2.140	83.8	82.0	78.1	64.9	68.7	72.4	69.5
5705.98	Fe I	4.61	-0.490	16.1
5753.12	Fe I	4.26	-0.690	26.6	20.5	26.8	15.2	19.2
5762.99	Fe I	4.21	-0.410	40.6	39.3	48.6	28.9	47.3	47.6	45.8
5775.06	Fe I	4.22	-1.300	14.9
5778.46	Fe I	2.59	-3.430	9.3	8.9
5806.72	Fe I	4.61	-0.950	8.9
5859.60	Fe I	4.55	-0.550	13.3	19.6	13.0
5862.35	Fe I	4.55	-0.330	25.6	27.8	32.1	23.7	24.1
5883.81	Fe I	3.96	-1.260	26.7	26.4	31.0
5930.17	Fe I	4.65	-0.140	36.0	25.6	30.4	21.7	26.0	40.6	28.5
5934.65	Fe I	3.93	-1.070	34.2	18.0	29.3	21.9	31.2
5952.72	Fe I	3.98	-1.340	14.2	14.1	17.8
5956.69	Fe I	0.86	-4.500	99.8	92.3	89.8	75.9	94.3	80.0	74.6
5976.79	Fe I	3.94	-1.330	22.5	27.4	26.5	...	33.4	...	24.2
5983.69	Fe I	4.55	-0.660	19.6	...	10.1
5984.83	Fe I	4.73	-0.260	...	17.3

Table 3—Continued

λ (Å)	Ion	χ_{exc} (eV)	$\log gf$ (dex)	S223 (mÅ)	S1814 (mÅ)	S810 (mÅ)	S1209 (mÅ)	S973 (mÅ)	S1305 (mÅ)	S1131 (mÅ)
6024.05	Fe I	4.55	0.030	56.5	44.5	53.0	45.3	45.7	41.1	54.6
6027.05	Fe I	4.07	-1.090	24.9	23.8	36.3	16.9	...	19.1	31.6
6055.99	Fe I	4.73	-0.370	16.1	21.7
6065.48	Fe I	2.61	-1.410	141.4	135.5	125.3	115.0	131.7	105.6	115.5
6078.50	Fe I	4.79	-0.330	17.8	13.5
6136.62	Fe I	2.45	-1.410	...	147.6	145.4	136.5	139.4	114.1	144.3
6136.99	Fe I	2.20	-2.930	54.2	...
6137.69	Fe I	2.59	-1.350	159.4	133.3	139.8	128.2	132.1	126.5	134.1
6151.62	Fe I	2.18	-3.370	48.8	50.3	45.0	33.3	47.0	22.9	36.4
6157.73	Fe I	4.07	-1.160	16.4	11.3	34.8	...	18.4
6165.36	Fe I	4.14	-1.470	6.2
6173.34	Fe I	2.22	-2.880	87.0	70.4	80.8	65.3	65.1	59.6	70.9
6180.20	Fe I	2.73	-2.650	40.7	38.3	34.3	21.5	43.0	26.8	33.1
6187.99	Fe I	3.94	-1.620	14.2
6191.56	Fe I	2.43	-1.420	150.3	145.7	145.1	135.2	143.4	121.7	140.9
6200.31	Fe I	2.61	-2.370	71.5	60.7	63.3	44.6	86.4	56.1	59.9
6240.65	Fe I	2.22	-3.170	47.2	39.1	52.7	32.1	42.6	29.4	33.2
6246.32	Fe I	3.60	-0.880	76.8	74.4	69.8	60.2	71.8	72.3	73.1
6252.55	Fe I	2.40	-1.770	148.6	140.1	122.8	119.2	118.8	116.8	127.5
6254.26	Fe I	2.28	-2.430	113.9	99.6	97.3	85.8	93.5	80.6	101.5
6265.13	Fe I	2.18	-2.540	111.9	97.2	106.3	89.2	122.0	83.3	95.5
6297.79	Fe I	2.22	-2.640	92.6	70.6	77.1	62.5	85.3	66.7	65.9
6301.51	Fe I	3.65	-0.718	76.3	66.8	72.1	61.9	...	61.6	73.6
6302.50	Fe I	3.69	-1.110	51.3	37.3	43.3	...	56.7
6311.50	Fe I	2.83	-3.140	13.6
6315.31	Fe I	4.14	-1.230	10.4
6315.81	Fe I	4.07	-1.610	10.8
6355.03	Fe I	2.84	-2.290	45.7	43.5	56.2	37.1	39.3	39.5	37.9
6380.75	Fe I	4.19	-1.380	10.6	12.0	11.6
6393.60	Fe I	2.43	-1.580	162.0	134.3	141.0	127.2	139.1	133.9	139.7
6408.03	Fe I	3.69	-1.020	50.7	54.0	53.5	45.4	63.8	53.8	53.2
6411.65	Fe I	3.65	-0.720	85.9	90.7	77.9	72.2	86.8	78.7	78.3
6421.35	Fe I	2.28	-2.010	120.3
6430.84	Fe I	2.18	-1.950	165.6	139.9	128.8	129.6	141.9	134.9	132.6
6475.63	Fe I	2.56	-2.940	49.5	...	41.7	26.0
6481.87	Fe I	2.28	-3.010	72.7	54.2	63.3	46.5	65.6	42.3	55.2
6494.98	Fe I	2.40	-1.240	...	172.2	159.2	153.1	166.6	149.0	152.3
6498.94	Fe I	0.96	-4.690	88.4	63.8	83.2	60.6	79.0	64.3	68.4
6546.24	Fe I	2.76	-1.540	125.0	117.4	108.5	95.8	122.0	89.8	104.0
6581.21	Fe I	1.48	-4.680	16.6	21.7	11.3	...
6592.91	Fe I	2.73	-1.470	127.1	117.5	119.3	111.4	117.7	102.3	117.5
6593.87	Fe I	2.43	-2.370	96.1	87.5	86.8	71.9	93.8	80.1	84.2
6608.02	Fe I	2.28	-3.930	...	9.8	11.1	8.4
6609.11	Fe I	2.56	-2.660	54.9	47.2	63.0	47.0	54.1	44.6	43.3
6625.02	Fe I	1.01	-5.370	38.0	20.5	36.6	23.0	23.0	...	22.5

Table 3—Continued

λ (Å)	Ion	χ_{exc} (eV)	$\log gf$ (dex)	S223 (mÅ)	S1814 (mÅ)	S810 (mÅ)	S1209 (mÅ)	S973 (mÅ)	S1305 (mÅ)	S1131 (mÅ)
6648.12	Fe I	1.01	-5.920	11.9	7.7
6703.57	Fe I	2.76	-3.060	19.4	18.0	16.2
6739.52	Fe I	1.56	-4.790	21.8
6750.15	Fe I	2.42	-2.580	90.9	79.7	81.3	68.4	87.2	63.2	77.0
6839.83	Fe I	2.56	-3.350	12.3	13.4	12.3
6855.18	Fe I	4.56	-0.740	17.9	17.7	13.8
6861.95	Fe I	2.42	-3.850	8.9
6978.85	Fe I	2.48	-2.450	96.4	75.3	93.6	65.8	73.3
6988.52	Fe I	2.40	-3.560	20.4	22.9	20.3
6999.88	Fe I	4.10	-1.460	13.8	11.6
7022.95	Fe I	4.19	-1.150	20.5	15.6
7038.22	Fe I	4.22	-1.200	22.0
7112.17	Fe I	2.99	-3.100	12.4
7130.92	Fe I	4.22	-0.750	29.4	26.4	26.2	28.8	34.0
7151.47	Fe I	2.48	-3.660	19.3	14.3	8.6
7179.99	Fe I	1.48	-4.750	28.4	24.2	11.2
7288.74	Fe I	4.22	-1.280	18.3
7411.16	Fe I	4.28	-0.280	40.0	40.8	69.3	31.6	40.0
7418.67	Fe I	4.14	-1.380	10.1
7445.75	Fe I	4.26	0.030	65.8	55.4	65.0	57.6	57.6
7461.52	Fe I	2.56	-3.530	22.8	17.0
7568.91	Fe I	4.28	-0.940	24.7	14.8	21.9
7583.79	Fe I	3.02	-1.890	67.2	61.8	71.5	50.4	56.3
7586.04	Fe I	4.31	-0.130	48.0	47.7	63.8	40.0	56.7
7742.72	Fe I	4.99	-0.420	24.0
7748.27	Fe I	2.95	-1.750	102.9	86.8	105.0	76.2	83.6
7780.57	Fe I	4.47	-0.040	62.9	54.5	37.0	45.4
4416.82	Fe II	2.77	-2.430	61.0	74.5
4491.40	Fe II	2.84	-2.600	71.0	69.6	...	70.7
4508.30	Fe II	2.84	-2.280	86.4	83.8	...	73.1	83.1
4555.89	Fe II	2.82	-2.170	100.2
4576.34	Fe II	2.83	-2.900	46.0	68.6	60.0
4583.84	Fe II	2.81	-2.020	...	122.0	98.0
4923.93	Fe II	2.88	-1.320	157.0	148.9	127.3	142.9	132.4	123.6	146.0
5018.45	Fe II	2.89	-1.220	...	166.5	146.9	155.0	...	146.0	167.6
5197.58	Fe II	3.23	-2.230	84.1	64.8	65.1	60.6	78.6	61.2	76.8
5234.63	Fe II	3.22	-2.220	82.3	77.3	73.0	62.3	58.8	72.5	80.8
5425.26	Fe II	3.00	-3.240	24.8	19.0	17.0	20.0	24.3
5534.85	Fe II	3.25	-2.640	35.0	49.8	45.2	42.4
6149.26	Fe II	3.89	-2.690	11.2	10.0	12.2
6247.56	Fe II	3.89	-2.360	27.7	25.1	37.0	20.0	25.5
6456.39	Fe II	3.90	-2.310	46.4	38.1
6516.08	Fe II	2.89	-3.450	33.9	40.0	...	29.1	35.6	40.7	42.3
5483.34	Co I	1.71	-1.490	58.7	30.1
5530.79	Co I	1.71	-2.060	27.2

Table 3—Continued

λ (Å)	Ion	χ_{exc} (eV)	$\log gf$ (dex)	S223 (mÅ)	S1814 (mÅ)	S810 (mÅ)	S1209 (mÅ)	S973 (mÅ)	S1305 (mÅ)	S1131 (mÅ)
6189.00	Co I	1.71	-2.450	9.5
6771.03	Co I	1.88	-1.970	14.7
7417.41	Co I	2.04	-2.070	10.0	6.0
5578.72	Ni I	1.68	-2.640	60.9	50.7	54.8	41.8	67.2	36.5	51.6
5587.86	Ni I	1.93	-2.140	...	57.2	57.4	37.4	56.7	34.0	...
5592.26	Ni I	1.95	-2.590	...	44.1	61.9	...	51.4	...	48.4
5748.35	Ni I	1.68	-3.260	21.8	21.5	20.2
5846.99	Ni I	1.68	-3.210	16.7	...	23.6	14.3	17.4
5892.87	Ni I	1.99	-2.340	66.6	62.5	71.5	51.8	64.7	35.5	66.5
6128.97	Ni I	1.68	-3.330	26.3	16.0	33.8	11.8	18.2
6176.81	Ni I	4.09	-0.529	15.0
6314.66	Ni I	1.93	-1.770	...	65.0	70.5
6482.80	Ni I	1.93	-2.630	29.4	28.8	29.5	19.8	...	24.4	22.1
6586.31	Ni I	1.95	-2.810	35.4	33.6	35.8	23.9	28.0	31.0	26.6
6643.63	Ni I	1.68	-2.300	117.8	100.2	102.1	88.2	97.4	88.0	94.0
6767.77	Ni I	1.83	-2.170	104.6	89.7	96.3	75.3	97.2	66.1	83.2
6772.31	Ni I	3.66	-0.987	11.7
7110.88	Ni I	1.93	-2.970	28.8	14.8
7122.20	Ni I	3.54	0.048	69.5	52.0	71.6	58.3	61.6	53.4	65.8
7261.92	Ni I	1.95	-2.700	65.9	52.2
7409.35	Ni I	3.80	-0.100	44.8
7414.50	Ni I	1.99	-2.570	62.2	55.9	54.7	46.0	48.7
7422.27	Ni I	3.63	-0.129	47.9	49.2	55.0	32.0	53.2
7574.05	Ni I	3.83	-0.580	16.5	10.6	20.6
7727.62	Ni I	3.68	-0.162	54.6	38.2	45.5	...	47.9
7748.89	Ni I	3.70	-0.130	40.5	40.1	37.6	42.4	41.9
7788.93	Ni I	1.95	-2.420	92.0	80.0	100.7	63.9	88.0	66.0	79.0
7797.59	Ni I	3.90	-0.180	34.1	26.7	22.3	26.6
5105.54	Cu I	1.39	-1.505	52.8	51.7	52.0	38.0	61.6	39.7	43.1
5782.12	Cu I	1.64	-1.780	18.2
4722.16	Zn I	4.03	-0.390	38.0	21.0	27.9	39.0
4810.54	Zn I	4.08	-0.170	34.0	49.9	34.2	39.0
4607.33	Sr I	0.00	0.280	...	34.2	28.0	16.0	22.7
4215.52	Sr II	0.00	-0.140	...	264.4	240.3	220.0
4398.01	Y II	0.13	-1.000	102.0	83.1
4854.87	Y II	0.99	-0.380	41.7	48.4
4883.69	Y II	1.08	0.070	67.1	68.5	68.4	66.7	64.0	66.0	68.6
5087.43	Y II	1.08	-0.170	49.6	47.2	34.0	43.2	60.0	42.0	52.8
5200.42	Y II	0.99	-0.570	54.0	43.2	42.0	42.2	45.9
5205.73	Y II	1.03	-0.340	47.0	...	38.0	...
6127.44	Zr I	0.15	-1.060	6.7
4554.04	Ba II	0.00	0.170	213.2
5853.70	Ba II	0.60	-1.010	98.9	89.3	76.2	89.3	84.3	95.3	103.2
6141.70	Ba II	0.70	-0.070	187.8	158.4	133.4	147.2	147.3	155.1	149.1
6496.90	Ba II	0.60	-0.380	175.6	160.8	137.7	155.9	148.6	146.4	147.7

Table 3—Continued

λ (Å)	Ion	χ_{exc} (eV)	$\log gf$ (dex)	S223 (mÅ)	S1814 (mÅ)	S810 (mÅ)	S1209 (mÅ)	S973 (mÅ)	S1305 (mÅ)	S1131 (mÅ)
4333.76	La II	0.17	-0.060	...	80.0
5122.99	La II	0.32	-0.850	35.2
6390.48	La II	0.32	-1.410	5.1	8.1
4486.91	Ce II	0.30	-0.360	24.4	25.5
4562.37	Ce II	0.48	0.330	...	21.1	24.3	41.3	40.5
4628.16	Ce II	0.52	0.260	...	22.2	30.4	31.6	30.6
4446.39	Nd II	0.20	-0.350	24.8
4462.99	Nd II	0.56	0.040	27.6
4959.12	Nd II	0.06	-0.800	32.0	32.0	25.6	27.4	42.0
5092.79	Nd II	0.38	-0.610	9.9	14.2
5212.35	Nd II	0.20	-0.960	10.7	21.0	11.2
5249.58	Nd II	0.98	0.200	...	19.0	20.3	23.6	≤ 29.0	34.2	19.5
4129.70	Eu II	0.00	0.220	145.0	114.0	98.0	123.8	125.0
6645.11	Eu II	1.38	0.120	9.0	8.0	11.0	13.4	...	≤ 20.0	17.0
5169.69	Dy II	0.10	-1.660	...	10.0

Table 4. Equivalent Widths For NGC 7099 RGB Stars

λ (Å)	Ion	χ_{exc} (eV)	$\log gf$ (dex)	S31 (mÅ)	S34 (mÅ)	S38 (mÅ)	S42 (mÅ)	S81 (mÅ)
6300.30	[O I]	0.00	-9.780	8.0	8.7	7.8	7.8	5.0
6363.78	[O I]	0.02	-10.300	3.4	...	3.3	...	6.0
7771.94	O I	9.15	0.369	6.5	3.7	4.2	7.9	4.3
7774.17	O I	9.15	0.223	7.5	...
5682.63	Na I	2.10	-0.700	...	9.0	12.2	...	10.0
5688.19	Na I	2.10	-0.420	11.1	15.0	21.6	...	15.0
5889.95	Na I	0.00	0.110	217.1	236.6	261.9	171.0	239.0
5895.92	Na I	0.00	-0.190	195.9	210.8	232.7	157.3	215.2
6160.75	Na I	2.00	-1.230	4.0
4057.52	Mg I	4.34	-1.200	65.2	67.3	47.3	51.5	41.3
4167.28	Mg I	4.34	-0.745	79.6	88.5	66.9	69.6	48.0
4703.00	Mg I	4.34	-0.440	89.4	96.5	84.8	77.9	57.8
5172.70	Mg I	2.71	-0.380	235.0	295.0	234.9	205.9	183.4
5183.62	Mg I	2.72	-0.160	267.5	328.0	264.6	237.9	204.4
5528.40	Mg I	4.34	-0.498	100.5	105.0	99.6	83.5	68.5
5711.09	Mg I	4.34	-1.724	23.9	28.8	18.5	16.9	9.8
3961.52	Al I	0.00	-0.340	176.4	227.8	242.9	146.2	192.2
6696.02	Al I	3.14	-1.340	...	5.0	4.0	...	6.0
3905.53	Si I	1.91	-1.040	258.7	282.0	250.1
4102.94	Si I	1.91	-3.140	94.1	100.8	101.1	88.0	87.8
5690.43	Si I	4.93	-1.870	4.3
5772.15	Si I	5.08	-1.750	...	4.9
5948.54	Si I	5.08	-1.230	17.1	18.0	17.5	14.9	14.4
6155.13	Si I	5.62	-0.760	6.1	8.6	9.1
6237.32	Si I	5.62	-1.010	...	5.7	4.4	...	4.8
7003.57	Si I	5.96	-0.830	5.5
7034.90	Si I	5.87	-0.880	5.2
7405.77	Si I	5.61	-0.820	9.6	15.6	12.6
7415.95	Si I	5.61	-0.730	9.0	11.3	10.5	7.2	6.8
7423.50	Si I	5.62	-0.580	13.7	21.4	19.9	9.1	13.3
7698.97	K I	0.00	-0.168	68.7	90.5	73.0	49.7	60.5
4289.37	Ca I	1.88	-0.300	73.9	85.6	...	73.0	55.4
4302.54	Ca I	1.90	0.280	88.3
4318.66	Ca I	1.90	-0.210	75.4	75.8	75.2	64.7	53.2
4425.44	Ca I	1.88	-0.338	62.0	75.8	67.8	56.5	60.5
4435.69	Ca I	1.89	-0.520	81.2	86.4	64.7	61.8	55.7
4454.79	Ca I	1.90	0.260	102.0	109.6	104.8	83.3	93.7
4578.56	Ca I	2.52	-0.558	17.0	22.0	15.3	11.6	19.1
5512.99	Ca I	2.93	-0.300	11.3	16.9	13.4
5581.96	Ca I	2.52	-0.710	24.8	34.0	22.0	19.5	15.0
5588.75	Ca I	2.52	0.210	69.2	76.1	71.2	60.3	57.4
5590.11	Ca I	2.52	-0.710	22.8	28.9	22.6	23.2	16.1
5594.46	Ca I	2.52	-0.050	56.9	65.1	59.7	49.1	46.6
5601.28	Ca I	2.52	-0.690	22.0	31.2	25.4	19.4	16.8
5857.45	Ca I	2.93	0.230	39.1	50.5	43.2	31.3	29.5

Table 4—Continued

λ (Å)	Ion	χ_{exc} (eV)	$\log gf$ (dex)	S31 (mÅ)	S34 (mÅ)	S38 (mÅ)	S42 (mÅ)	S81 (mÅ)
6161.30	Ca I	2.52	-1.030	...	9.5	5.8
6162.17	Ca I	1.90	-0.090	101.5	117.2	108.3	82.7	86.9
6166.44	Ca I	2.52	-0.900	8.4	12.2	9.4	...	6.7
6169.04	Ca I	2.52	-0.540	19.3	24.9	16.5	17.8	...
6169.56	Ca I	2.52	-0.270	31.9	39.1	27.6	22.5	17.5
6471.66	Ca I	2.52	-0.590	26.1	31.2	25.6	21.1	14.7
6493.78	Ca I	2.52	0.140	50.9	61.8	51.2	35.3	38.5
6499.65	Ca I	2.54	-0.590	...	37.3	...	30.6	...
6717.68	Ca I	2.71	-0.610	23.2	29.1	26.7	18.6	15.5
7148.15	Ca I	2.71	0.218	59.3	69.4	65.1	49.2	42.8
4246.82	Sc II	0.32	0.242	130.5	149.1	159.9	124.0	133.9
4314.08	Sc II	0.62	-0.100	101.7	114.8
4320.73	Sc II	0.60	-0.260	96.6	105.0	114.5	87.0	105.1
4670.41	Sc II	1.36	-0.580	48.9	56.2	52.4	32.3	34.9
5526.79	Sc II	1.77	0.130	51.5	59.9	61.1	36.4	42.0
5657.90	Sc II	1.51	-0.500	40.0	51.6	47.8	27.1	29.7
5667.15	Sc II	1.50	-1.240	11.0	15.8	16.5
5669.04	Sc II	1.50	-1.120	12.8	21.8	18.2
5684.20	Sc II	1.51	-1.080	15.3	22.7	22.1	...	13.5
6245.64	Sc II	1.51	-1.130	17.3	20.2	17.0	...	7.0
6604.59	Sc II	1.36	-1.310	11.4	18.0	16.1	7.8	...
3924.53	Ti I	0.02	-0.940	47.9	36.0	26.3
3958.22	Ti I	0.05	-0.160	74.5	73.1	73.3
3998.64	Ti I	0.05	-0.050	87.6	71.6	71.7
4512.74	Ti I	0.84	-0.480	25.2	32.6	25.5	13.0	11.1
4518.03	Ti I	0.83	-0.230	30.6	41.3	30.0	22.3	19.1
4533.25	Ti I	0.85	0.480	67.3	78.2	71.5	56.2	57.3
4534.78	Ti I	0.84	0.280	58.5	67.9	61.9	48.1	42.7
4548.77	Ti I	0.83	-0.350	32.4	36.6	29.4	25.5	16.7
4555.49	Ti I	0.85	-0.490	20.1	33.9	23.4	21.7	10.1
4681.92	Ti I	0.05	-1.070	43.9	55.3	48.0	26.0	21.6
4981.74	Ti I	0.85	0.500	77.7	88.0	81.1	65.1	60.7
4999.51	Ti I	0.83	0.250	62.4	77.3	69.7	53.1	45.5
5022.87	Ti I	0.83	-0.430	31.3	40.7	32.0	16.4	16.9
5039.96	Ti I	0.02	-1.130	46.6	57.0	47.5	29.9	21.5
5173.75	Ti I	0.00	-1.120	47.2	61.0	54.3	32.5	29.7
5210.39	Ti I	0.05	-0.880	61.5	70.5	61.3	43.6	38.1
5866.45	Ti I	1.07	-0.840	10.6	13.3	8.0
5953.16	Ti I	1.89	-0.329	4.7
5965.83	Ti I	1.88	-0.409	5.0	4.2
6258.10	Ti I	1.44	-0.355	8.5	13.3	9.7	5.2	...
6258.71	Ti I	1.46	-0.240	14.5	17.6	10.6	...	5.4
6261.10	Ti I	1.43	-0.479	7.3	11.0	11.0
6743.12	Ti I	0.90	-1.630	2.6
3900.54	Ti II	1.13	-0.450	139.3	118.4	146.9

Table 4—Continued

λ (Å)	Ion	χ_{exc} (eV)	$\log gf$ (dex)	S31 (mÅ)	S34 (mÅ)	S38 (mÅ)	S42 (mÅ)	S81 (mÅ)
3987.61	Ti II	0.61	-2.730	57.8	44.8	50.8
4012.39	Ti II	0.57	-1.610	109.8	129.4	135.8	97.5	...
4028.35	Ti II	1.89	-0.870	72.6	81.3	80.4	60.3	69.3
4300.05	Ti II	1.18	-0.490	127.4
4301.93	Ti II	1.16	-1.200	101.1
4312.86	Ti II	1.18	-1.160	104.4
4395.03	Ti II	1.08	-0.510	151.7	155.9	162.9	134.8	139.2
4399.77	Ti II	1.24	-1.290	102.8	112.0	115.0	94.4	100.1
4417.72	Ti II	1.16	-1.160	106.7	112.8	118.2	88.6	99.2
4443.81	Ti II	1.08	-0.700	128.5	140.5	148.4	115.3	129.5
4468.51	Ti II	1.13	-0.600	128.2	140.5	151.9	114.8	131.1
4501.28	Ti II	1.12	-0.760	123.3	134.4	147.1	114.6	128.6
4533.97	Ti II	1.24	-0.640	139.3	138.1	160.0	115.6	138.0
4563.77	Ti II	1.22	-0.820	118.0	130.2	137.1	102.3	114.2
4571.98	Ti II	1.57	-0.340	123.5	129.6	142.7	105.8	116.7
4583.41	Ti II	1.16	-2.870	20.1	35.2	29.6	18.9	13.1
4589.95	Ti II	1.24	-1.650	81.0	91.3	94.9	63.1	76.9
4657.20	Ti II	1.24	-2.320	50.9	57.5	58.5	31.1	39.1
4708.67	Ti II	1.24	-2.370	43.1	56.1	55.7	35.7	30.8
4762.78	Ti II	1.08	-2.710	30.6	38.8	35.7	21.6	17.2
4798.54	Ti II	1.08	-2.670	39.6	51.9	50.1	25.5	29.6
4865.62	Ti II	1.12	-2.810	28.0	42.9	39.0	20.8	25.8
4911.20	Ti II	3.12	-0.340	21.5	21.3	18.7	...	15.7
5185.91	Ti II	1.89	-1.460	53.9	58.5	58.2	35.3	40.5
4111.77	V I	0.30	0.408	28.6	41.5	24.6	14.8	10.6
6090.22	V I	1.08	-0.062	...	5.0
6251.82	V I	0.29	-1.340	...	2.5
4254.33	Cr I	0.00	-0.110	123.7	134.5	132.5	111.4	114.7
4274.79	Cr I	0.00	-0.230	127.6	151.9	137.3	112.1	107.9
4289.72	Cr I	0.00	-0.361	110.1	107.8
4545.96	Cr I	0.94	-1.380	24.0	33.6	27.4	18.9	12.9
4600.76	Cr I	1.00	-1.280	27.8	34.4	27.2	15.7	8.6
4613.37	Cr I	0.96	-1.670	...	19.2	16.0
4616.13	Cr I	0.98	-1.210	28.0	38.3	35.1	18.1	12.8
4626.18	Cr I	0.97	-1.340	25.0	35.4	24.7	14.5	14.1
4652.17	Cr I	1.00	-1.030	35.4	46.7	38.9	26.2	23.2
5206.04	Cr I	0.94	0.030	99.8	117.5	106.8	88.7	80.4
5409.80	Cr I	1.03	-0.710	56.8	71.8	61.0	41.8	33.8
4030.75	Mn I	0.00	-0.470	154.9	159.7	161.7	132.0	127.9
4033.06	Mn I	0.00	-0.620	137.8	146.3	150.3	107.0	112.3
4754.04	Mn I	2.28	-0.090	26.0	34.1	24.2	12.9	11.8
4783.42	Mn I	2.30	0.042	25.6	37.5	32.8	24.5	20.6
4823.51	Mn I	2.32	0.140	35.0	40.7	38.1	20.4	20.1
5394.69	Mn I	0.00	-3.503	...	7.9
6021.80	Mn I	3.08	0.034	...	7.6	8.6

Table 4—Continued

λ (Å)	Ion	χ_{exc} (eV)	$\log gf$ (dex)	S31 (mÅ)	S34 (mÅ)	S38 (mÅ)	S42 (mÅ)	S81 (mÅ)
3895.67	Fe I	0.11	-1.670	168.0
3899.72	Fe I	0.09	-1.530	181.4	170.7
3902.96	Fe I	1.56	-0.470	133.1
3906.49	Fe I	0.11	-2.240	150.5	139.5
3916.74	Fe I	3.24	-0.560	40.9
3920.27	Fe I	0.12	-1.750	136.4	146.4
3922.92	Fe I	0.05	-1.650	172.8	142.8	166.9
3949.96	Fe I	2.18	-1.160	85.3	75.3	77.3
4005.24	Fe I	1.56	-0.610	143.5	158.2	158.3	124.2	127.9
4063.59	Fe I	1.56	0.060	165.5	162.7
4071.74	Fe I	1.61	-0.020	164.2	151.8
4118.55	Fe I	3.57	0.140	75.5	87.8	76.6	...	63.9
4132.06	Fe I	1.61	-0.820	123.9	...
4143.87	Fe I	1.56	-0.620	142.7	147.2	155.3	123.4	135.8
4147.67	Fe I	1.49	-2.100	91.1	95.0	97.6	76.6	68.6
4174.92	Fe I	0.91	-2.970	...	101.3	...	70.5	...
4181.75	Fe I	2.83	-0.370	82.8	97.1	92.3	72.5	66.8
4187.05	Fe I	2.45	-0.550	102.7	105.1	109.6	88.3	94.6
4187.81	Fe I	2.43	-0.550	101.4	115.6	111.3	96.7	90.8
4199.10	Fe I	3.05	0.160	91.7	100.6	98.6	...	83.8
4202.04	Fe I	1.49	-0.710	137.6	148.3	153.3	116.8	132.9
4222.22	Fe I	2.45	-0.970	82.2	87.9	89.8	73.6	66.8
4227.44	Fe I	3.33	0.270	97.6
4233.61	Fe I	2.48	-0.600	95.7	101.2	99.6	77.5	81.7
4235.95	Fe I	2.43	-0.340	130.4	102.2	109.2
4250.13	Fe I	2.47	-0.404	102.1	108.6	109.7	81.0	89.7
4250.80	Fe I	1.56	-0.720	141.6
4260.49	Fe I	2.40	0.140	127.2	134.5	134.8	114.3	114.3
4271.16	Fe I	2.45	-0.350	125.3	...	120.2	...	94.7
4271.77	Fe I	1.49	-0.160	160.7	153.8
4282.41	Fe I	2.18	-0.780	100.9	118.0	104.9	88.8	83.8
4299.25	Fe I	2.43	-0.350	101.7
4307.91	Fe I	1.56	-0.070	170.7
4325.77	Fe I	1.61	0.010	...	199.3	...	152.5	161.6
4337.05	Fe I	1.56	-1.690	99.3	109.7	105.8	79.3	82.2
4375.94	Fe I	0.00	-3.030	129.2	139.1	143.3	...	114.0
4383.56	Fe I	1.49	0.200	174.4
4404.76	Fe I	1.56	-0.140	169.1	190.4	...	147.0	155.7
4415.13	Fe I	1.61	-0.610	144.3	155.3	156.8	126.0	124.8
4430.62	Fe I	2.22	-1.660	72.5	76.5	68.1	50.7	45.9
4442.35	Fe I	2.20	-1.250	90.9	104.8	97.7	75.4	70.6
4447.73	Fe I	2.22	-1.340	83.3	92.0	85.8	63.6	64.1
4461.66	Fe I	0.09	-3.210	120.5	133.2	133.7	100.4	101.1
4489.75	Fe I	0.12	-3.970	91.8	103.5	99.6	68.0	64.0
4494.57	Fe I	2.20	-1.140	93.7	104.2	101.4	75.6	73.6

Table 4—Continued

λ (Å)	Ion	χ_{exc} (eV)	$\log gf$ (dex)	S31 (mÅ)	S34 (mÅ)	S38 (mÅ)	S42 (mÅ)	S81 (mÅ)
4531.16	Fe I	1.49	-2.150	89.3	103.4	101.7	75.4	73.6
4592.66	Fe I	1.56	-2.450	77.2	87.1	...	57.3	49.4
4602.95	Fe I	1.49	-2.220	94.2	99.5	96.6	67.1	67.0
4625.05	Fe I	3.24	-1.348	20.2	33.7	24.6	16.6	15.7
4788.77	Fe I	3.24	-1.806	7.8	12.1	5.8
4871.33	Fe I	2.86	-0.360	89.3	101.3	99.0	78.9	73.9
4872.14	Fe I	2.88	-0.570	79.7	89.5	89.3	67.2	64.6
4891.50	Fe I	2.85	-0.110	103.4	108.3	108.6	85.9	83.6
4919.00	Fe I	2.86	-0.340	91.1	101.7	94.2	77.7	76.5
4920.51	Fe I	2.83	0.150	116.6	134.3	127.9	97.8	97.9
4957.61	Fe I	2.81	0.230	124.7	139.1	134.3	108.2	111.6
5083.34	Fe I	0.96	-2.960	92.5	103.9	103.1	70.9	67.2
5166.28	Fe I	0.00	-4.200	...	108.5	...	71.3	61.1
5171.61	Fe I	1.48	-1.790	110.8	121.2	123.3	96.9	96.9
5192.35	Fe I	3.00	-0.420	82.1	88.8	86.5	65.5	61.5
5194.95	Fe I	1.56	-2.090	95.1	106.7	104.3	74.4	72.0
5198.72	Fe I	2.22	-2.140	48.0	57.5	51.2	34.5	26.6
5216.28	Fe I	1.61	-2.150	88.3	100.4	95.3	72.8	66.3
5217.40	Fe I	3.21	-1.070	35.5	42.6	33.7	19.2	22.5
5227.19	Fe I	1.56	-1.350	119.8
5232.95	Fe I	2.94	-0.100	102.0	109.9	107.9	90.4	86.8
5269.55	Fe I	0.86	-1.320	169.5	146.4	155.2
5393.18	Fe I	3.24	-0.720	53.8	61.4	52.9	38.0	34.9
5405.79	Fe I	0.99	-1.840	138.6	151.1	153.1	123.5	125.2
5410.92	Fe I	4.47	0.400	29.4	37.6	30.6	21.6	21.0
5415.21	Fe I	4.39	0.640	45.0	52.0	45.5	35.0	34.1
5424.08	Fe I	4.32	0.510	50.9	62.4	55.6	39.6	40.1
5434.53	Fe I	1.01	-2.130	127.1	140.0	142.2	115.1	110.5
5445.05	Fe I	4.39	-0.030	22.2	26.8	29.0	21.3	15.4
5466.39	Fe I	4.37	-0.620	10.4	11.6	7.6	...	8.1
5473.90	Fe I	4.15	-0.690	8.9	12.6	8.2	...	4.8
5487.77	Fe I	4.14	-0.620	11.8	13.5	9.5	...	5.7
5497.52	Fe I	1.01	-2.830	100.1	113.4	110.8	82.7	72.3
5501.46	Fe I	0.96	-3.050	92.2	104.7	103.3	71.6	61.8
5506.79	Fe I	0.99	-2.790	104.3	115.4	114.9	83.4	78.6
5554.88	Fe I	4.55	-0.350	7.8	9.6	6.5
5567.39	Fe I	2.61	-2.670	8.4	17.0	10.8
5569.62	Fe I	3.42	-0.486	52.5	59.3	51.8	38.8	37.8
5572.84	Fe I	3.40	-0.275	67.6	76.2	65.4	50.3	45.6
5576.09	Fe I	3.43	-0.920	33.1	42.4	36.0	21.3	20.0
5586.76	Fe I	3.37	-0.140	73.8	83.4	81.3	60.5	59.1
5624.54	Fe I	3.42	-0.755	40.5	47.6	40.8	30.6	23.9
5662.52	Fe I	4.18	-0.570	12.6	18.2	13.1	...	8.8
5679.02	Fe I	4.65	-0.820	...	4.8
5701.54	Fe I	2.56	-2.140	30.0	33.0	24.8	13.2	7.9

Table 4—Continued

λ (Å)	Ion	χ_{exc} (eV)	$\log gf$ (dex)	S31 (mÅ)	S34 (mÅ)	S38 (mÅ)	S42 (mÅ)	S81 (mÅ)
5753.12	Fe I	4.26	-0.690	6.3	10.4	5.4
5762.99	Fe I	4.21	-0.410	17.1	24.6	17.4	...	10.3
5859.60	Fe I	4.55	-0.550	6.7	5.4
5862.35	Fe I	4.55	-0.330	7.7	13.6	8.8
5883.81	Fe I	3.96	-1.260	...	5.8
5930.17	Fe I	4.65	-0.140	8.9	11.4	10.3
5934.65	Fe I	3.93	-1.070	4.7	10.7
5956.69	Fe I	0.86	-4.500	18.1	25.8	20.8	7.7	6.7
5983.69	Fe I	4.55	-0.660	...	6.7	4.8
5984.83	Fe I	4.73	-0.260	...	9.7	5.2
6024.05	Fe I	4.55	0.030	18.6	24.6	18.9	8.8	13.5
6027.05	Fe I	4.07	-1.090	4.5	7.8
6065.48	Fe I	2.61	-1.410	54.9	71.1	65.1	42.9	34.5
6078.50	Fe I	4.79	-0.330	8.1
6136.62	Fe I	2.45	-1.410	76.5	88.0	83.7	62.8	52.6
6136.99	Fe I	2.20	-2.930	17.4	23.4	19.0	10.4	...
6137.69	Fe I	2.59	-1.350	67.4	80.8	72.8	53.3	43.0
6151.62	Fe I	2.18	-3.370	...	10.8	9.3
6157.73	Fe I	4.07	-1.160	...	7.1
6173.34	Fe I	2.22	-2.880	17.5	25.8	21.1	8.6	...
6180.20	Fe I	2.73	-2.650	...	10.3	4.3
6191.56	Fe I	2.43	-1.420	75.5	86.2	80.7	58.7	48.9
6200.31	Fe I	2.61	-2.370	15.2	20.9	15.6	15.2	...
6240.65	Fe I	2.22	-3.170	7.1	10.6	8.9
6246.32	Fe I	3.60	-0.880	27.9	35.3	25.5	15.0	13.2
6252.55	Fe I	2.40	-1.770	63.4	78.7	70.2	49.5	44.7
6254.26	Fe I	2.28	-2.430	36.9
6265.13	Fe I	2.18	-2.540	35.2	46.1	38.6	22.4	14.7
6297.79	Fe I	2.22	-2.640	18.6	30.6	22.4	14.6	12.5
6301.51	Fe I	3.65	-0.718	26.7	35.2	28.5	19.4	14.9
6302.50	Fe I	3.69	-1.110	10.4	15.4	11.3	12.6	...
6355.03	Fe I	2.84	-2.290	9.2	15.6	11.2
6393.60	Fe I	2.43	-1.580	72.1	84.0	75.3	54.4	49.3
6408.03	Fe I	3.69	-1.020	17.3	18.9	13.9	...	5.9
6411.65	Fe I	3.65	-0.720	33.5	48.0	36.5	27.3	21.7
6421.35	Fe I	2.28	-2.010	59.5	72.0	62.0	43.3	31.8
6430.84	Fe I	2.18	-1.950	67.8	82.3	72.0	45.6	41.0
6475.63	Fe I	2.56	-2.940	5.1	11.6	7.9
6481.87	Fe I	2.28	-3.010	11.6	18.7	11.1
6494.98	Fe I	2.40	-1.240	90.2	101.5	96.6	75.4	69.8
6498.94	Fe I	0.96	-4.690	11.5	20.8	17.3	5.0	...
6592.91	Fe I	2.73	-1.470	49.2	63.6	55.0	37.9	30.5
6593.87	Fe I	2.43	-2.370	23.9	37.9	27.2	15.8	...
6609.11	Fe I	2.56	-2.660	11.1	17.2	10.5
6750.15	Fe I	2.42	-2.580	21.8	27.2	20.9	11.3	...

Table 4—Continued

λ (Å)	Ion	χ_{exc} (eV)	$\log gf$ (dex)	S31 (mÅ)	S34 (mÅ)	S38 (mÅ)	S42 (mÅ)	S81 (mÅ)
6843.65	Fe I	4.55	-0.830	4.8
6855.18	Fe I	4.56	-0.740	...	4.1
6978.85	Fe I	2.48	-2.450	23.9	29.4	23.2	...	6.0
6999.88	Fe I	4.10	-1.460	3.5
7038.22	Fe I	4.22	-1.200	...	3.8
7130.92	Fe I	4.22	-0.750	...	12.7	...	4.5	6.6
7411.16	Fe I	4.28	-0.280	13.9	18.3	13.3	10.6	7.6
7445.75	Fe I	4.26	0.030	26.5	29.8	20.4	19.8	17.3
7495.06	Fe I	4.22	0.230	36.5	43.6	29.2	28.8	26.3
7568.91	Fe I	4.28	-0.940	7.2	9.3
7583.79	Fe I	3.02	-1.890	16.5	26.5	16.9	12.9	...
7586.04	Fe I	4.31	-0.130	17.1	22.0	21.5	13.0	...
7742.72	Fe I	4.99	-0.420	...	7.7	6.9
7748.27	Fe I	2.95	-1.750	27.4	38.0	29.7	16.8	15.5
7780.57	Fe I	4.47	-0.040	16.8	22.7	19.6	12.7	9.6
4178.86	Fe II	2.57	-2.530	60.1	74.7	76.9	52.5	60.2
4233.17	Fe II	2.57	-2.000	98.7	94.4	107.7	73.3	101.6
4416.82	Fe II	2.77	-2.430	52.1	56.9	56.7	38.9	45.2
4491.40	Fe II	2.84	-2.600	40.5	53.2	45.9	27.3	39.3
4508.30	Fe II	2.84	-2.280	59.3	64.9	71.8	47.0	51.8
4555.89	Fe II	2.82	-2.170	59.9	70.8	72.6	51.4	56.5
4576.34	Fe II	2.83	-2.900	27.7	39.1	34.2	18.8	27.0
4583.84	Fe II	2.81	-2.020	84.4	90.8	97.5	77.8	88.2
4923.93	Fe II	2.88	-1.320	109.5	113.9	122.4	87.1	110.2
5018.45	Fe II	2.89	-1.220	120.6	126.8	139.7	104.1	122.9
5197.58	Fe II	3.23	-2.230	45.5	52.0	53.2	40.4	41.9
5234.63	Fe II	3.22	-2.220	51.5	55.8	57.3	35.2	42.2
5414.08	Fe II	3.22	-3.620	4.0	6.2	7.0	6.1	...
5425.26	Fe II	3.00	-3.240	8.1	16.6	10.8	...	7.8
5534.85	Fe II	3.25	-2.640	19.0	27.7	26.9	12.0	19.5
5991.38	Fe II	3.15	-3.570	...	9.6
6149.26	Fe II	3.89	-2.690	...	7.1	8.8	...	8.6
6247.56	Fe II	3.89	-2.360	13.4	16.7	16.4	9.7	10.0
6369.46	Fe II	2.89	-4.200	3.2
6416.92	Fe II	3.89	-2.690	...	6.2	7.2
6516.08	Fe II	2.89	-3.450	...	24.9	22.9
3873.11	Co I	0.43	-0.666	...	103.7	111.6
4121.31	Co I	0.92	-0.315	93.4	100.7	95.9	83.0	77.7
4401.55	Ni I	3.19	0.084	46.9	...	50.6	40.9	32.2
5578.72	Ni I	1.68	-2.640	8.8	15.1	9.0
5587.86	Ni I	1.93	-2.140	10.1	15.0	12.3
5592.26	Ni I	1.95	-2.590	10.4	13.4	9.4
5892.87	Ni I	1.99	-2.340	16.0
6482.80	Ni I	1.93	-2.630	10.6	7.6	8.9
6586.31	Ni I	1.95	-2.810	...	6.3	...	7.0	...

Table 4—Continued

λ (Å)	Ion	χ_{exc} (eV)	$\log gf$ (dex)	S31 (mÅ)	S34 (mÅ)	S38 (mÅ)	S42 (mÅ)	S81 (mÅ)
6643.63	Ni I	1.68	-2.300	30.1	44.9	33.4	18.2	14.2
6767.77	Ni I	1.83	-2.170	26.4	35.0	30.5	17.1	...
7122.20	Ni I	3.54	0.048	33.1	31.4	31.2	23.5	27.0
7409.35	Ni I	3.80	-0.100	...	16.3	13.3
7414.50	Ni I	1.99	-2.570	13.8	18.2	13.6
7422.27	Ni I	3.63	-0.129	13.1	23.0	17.0	8.8	12.5
7574.05	Ni I	3.83	-0.580	...	7.5
7727.62	Ni I	3.68	-0.162	14.6	16.3	14.9	11.4	...
7748.89	Ni I	3.70	-0.130	13.8	15.5	12.2	8.3	6.6
7788.93	Ni I	1.95	-2.420	20.2	31.0	21.3	13.6	11.6
7797.59	Ni I	3.90	-0.180	9.6	10.3	11.3
5105.54	Cu I	1.39	-1.505	6.3	10.1	8.0
4722.16	Zn I	4.03	-0.390	16.6	24.3	21.5	14.6	21.7
4810.54	Zn I	4.08	-0.170	29.5	29.0	29.0	22.1	19.3
4077.71	Sr II	0.00	0.170	179.3	190.4	210.6	159.7	180.8
4215.52	Sr II	0.00	-0.140	173.6	187.0	195.4	150.7	158.9
3950.36	Y II	0.10	-0.490	57.9	66.4	69.8	59.7	58.7
4398.01	Y II	0.13	-1.000	41.5	44.7	47.6	31.1	26.2
4883.69	Y II	1.08	0.070	32.9	40.4	42.2	28.4	27.0
5087.43	Y II	1.08	-0.170	26.1	29.8	26.1	14.0	14.2
5200.42	Y II	0.99	-0.570	18.5	17.2	17.3	9.5	14.9
5205.73	Y II	1.03	-0.340	26.0	25.0	13.3	13.0	...
4161.21	Zr II	0.71	-0.720	35.2	47.0	44.3	27.7	27.7
4208.99	Zr II	0.71	-0.460	38.1	45.8	44.4	33.0	32.7
4317.32	Zr II	0.71	-1.380	11.6	14.8	14.9	12.5	...
4496.97	Zr II	0.71	-0.590	31.9
4554.04	Ba II	0.00	0.170	148.2	160.0	170.2	125.3	140.8
5853.70	Ba II	0.60	-1.010	41.1	52.4	52.4	26.2	31.3
6141.70	Ba II	0.70	-0.070	86.0	99.4	106.3	62.8	82.3
6496.90	Ba II	0.60	-0.380	86.9	99.0	107.9	66.8	72.0
3988.52	La II	0.40	0.210	8.1	26.8	23.4	...	17.1
3995.75	La II	0.17	-0.060	...	31.5	23.8	17.5	16.5
4086.71	La II	0.00	-0.070	22.4	34.0	32.0	19.8	26.2
4123.23	La II	0.32	0.130	12.2	28.2	23.7	18.3	...
4333.76	La II	0.17	-0.060	25.3	39.4	32.2	25.4	11.3
4083.23	Ce II	0.70	0.240	...	9.3
4120.84	Ce II	0.32	-0.240	7.4
4222.60	Ce II	0.12	-0.180	11.8	9.4	12.6
4418.79	Ce II	0.86	0.310	...	8.2	3.2
4486.91	Ce II	0.30	-0.360	9.7
4562.37	Ce II	0.48	0.330	8.5	12.1	13.7	9.9	...
4628.16	Ce II	0.52	0.260	9.8	11.0	10.6
3973.27	Nd II	0.63	0.360	...	16.0
4021.34	Nd II	0.32	-0.100	18.5	13.8	19.3
4061.09	Nd II	0.47	0.550	31.7	35.1	37.8	22.2	20.6

Table 4—Continued

λ (Å)	Ion	χ_{exc} (eV)	$\log gf$ (dex)	S31 (mÅ)	S34 (mÅ)	S38 (mÅ)	S42 (mÅ)	S81 (mÅ)
4069.27	Nd II	0.06	-0.570	...	9.2	13.4	11.5	...
4109.46	Nd II	0.32	0.350	27.6	44.6	46.5	19.5	15.4
4232.38	Nd II	0.06	-0.470	9.0	12.1	20.2
4446.39	Nd II	0.20	-0.350	13.4	16.4	13.1	6.1	...
4462.99	Nd II	0.56	0.040	18.3	13.2	12.5
4959.12	Nd II	0.06	-0.800	...	11.7	9.7
5092.79	Nd II	0.38	-0.610	...	8.2	8.4
5212.35	Nd II	0.20	-0.960	6.3
5249.58	Nd II	0.98	0.200	5.8
4318.94	Sm II	0.28	-0.270	8.8
4537.95	Sm II	0.48	-0.230	6.4
3907.11	Eu II	0.21	0.170	31.0	31.1	43.5	27.0	22.0
3971.96	Eu II	0.21	0.270	...	21.3	62.0
4129.70	Eu II	0.00	0.220	55.2	75.4	77.8	40.3	37.0
6645.11	Eu II	1.38	0.120	...	6.7
3869.86	Dy II	0.00	-0.940	...	20.4
3996.69	Dy II	0.59	-0.190	5.7
4103.31	Dy II	0.10	-0.370	24.0	24.7	30.7	14.7	6.9

Table 5. Deduced Slopes for Fe I Line-by-Line Abundances

ID	Fe I vs EP (dex eV ⁻¹)	Fe I vs (W_λ/λ) (dex)	Fe I vs λ (dex Å ⁻¹)
NGC 2419			
S1131	−0.042	0.010	−0.118e−4
S1305	−0.046	−0.075	0.168e−4
S1209	−0.050	−0.001	0.451e−4
S973	−0.038	0.045	0.093e−4
S1814	−0.083	−0.001	0.169e−4
S223	−0.079	0.077	−0.136e−4
NGC 7099			
S31	−0.041	0.008	−0.022e−4
S34	−0.042	0.008	−0.173e−4
S38	−0.042	0.017	−0.153e−4
S42	−0.055	0.012	−0.031e−4
S81	−0.047	0.009	−0.087e−5

Table 6. Abundances for Red Giant Members of NGC 2419

ID ^a Species	S1131 [X/Fe] (dex)	σ^b (dex)	N ^c	S1305 [X/Fe] (dex)	σ^b (dex)	N	S1209 [X/Fe] (dex)	σ^b (dex)	N	S973 [X/Fe] (dex)	σ^b (dex)	N	S810 [X/Fe] (dex)	σ^b (dex)	N	S1814 [X/Fe] (dex)	σ^b (dex)	N	S223 [X/Fe] (dex)	σ^b (dex)	N	
C ^d	-0.81	...	1	-0.26	0.30	1	-0.73	...	1	-0.90	...	1	-0.79	...	1
O I	0.67	...	1	0.71	0.03	2
Na I	-0.04	0.19	2	0.54	0.15	2	0.23	...	1	0.06	0.13	2	-0.42	0.09	3	-0.04	...	1	0.29	0.01	2	
Mg I	-0.47	0.17	5 ^e	0.32	0.15	5	0.62	0.18	3	0.46	0.20	3	0.32	0.22	3	0.55	0.19	5	0.30	0.22	5	
Al I ^f	0.45	...	1
Si I	0.56	0.16	13	0.54	0.18	4	0.43	0.32	4	0.33	0.17	5	0.30	0.17	4	
K I	1.13	...	1	0.36	...	1	0.47	...	1	0.45	...	1	0.49	...	1	0.55	...	1	
Ca I	0.23	0.18	18	0.21	0.22	15	0.20	0.14	14	0.17	0.22	15	0.05	0.14	11	0.12	0.17	18	0.08	0.16	14	
Sc II	0.32	0.08	7	0.15	0.20	7	0.08	0.13	6	-0.02	0.16	7	-0.01	0.08	7	0.08	0.12	8	0.19	0.07	7	
Ti I	0.16	0.17	23	0.18	0.19	10	0.06	0.15	17	0.08	0.21	9	0.00	0.17	14	0.15	0.16	23	0.17	0.13	19	
Ti II	0.34	0.33	9	0.28	0.09	4	0.38	0.16	10	0.08	0.16	3	0.02	0.27	7	0.40	0.14	7	0.25	0.27	5	
V I	0.03	0.15	4	0.18	0.43	2	0.08	0.13	3	0.01	0.07	3	0.03	0.07	3	-0.08	0.11	4	-0.07	0.14	9	
Cr I	-0.08	0.22	7	-0.37	0.25	2	-0.23	0.13	6	-0.25	0.03	2	-0.31	0.08	4	-0.20	0.14	6	-0.18	0.16	5	
Mn I	-0.24	0.16	7	-0.28	0.09	5	-0.27	0.18	6	-0.18	0.24	4	-0.39	0.12	6	-0.25	0.09	6	-0.33	0.11	6	
Fe I ^g	-1.95	0.15	108	-2.17	0.18	71	-2.20	0.10	75	-1.98	0.17	67	-2.00	0.12	78	-2.04	0.14	93	-2.09	0.15	91	
Fe II	-0.12	0.21	11	-0.05	0.17	8	-0.01	0.21	9	-0.11	0.26	6	-0.01	0.15	6	-0.08	0.20	14	-0.02	0.20	12	
Co I	0.03	...	1	0.04	...	1	0.21	0.18	3	0.10	0.01	2	
Ni I	-0.04	0.19	18	-0.05	0.22	13	-0.08	0.15	11	-0.08	0.25	14	0.02	0.26	13	-0.07	0.20	21	-0.07	0.18	21	
Cu I	-0.65	...	1	-0.55	...	1	-0.63	...	1	-0.48	...	1	-0.63	...	1	-0.52	...	1	-0.79	0.02	2	
Zn I	-0.14	0.13	2	-0.23	0.02	2	-0.16	0.30	2	-0.27	0.18	2	
Sr I	-0.30	...	1	-0.31	...	1	-0.28	...	1	-0.04	...	1	
Sr II	-0.18	...	1	-0.15	...	1	-0.02	...	1	
Y II	-0.46	0.09	3	-0.42	0.13	3	-0.37	0.10	5	-0.43	0.07	2	-0.56	0.21	4	-0.43	0.15	4	-0.27	0.30	4	
Zr I	0.45	...	1	
Ba II	-0.18	0.05	4	-0.03	0.05	3	-0.08	0.13	3	-0.22	0.16	3	-0.41	0.13	3	-0.25	0.11	3	-0.01	0.23	3	
La II	-0.09	...	1	0.38	...	1	-0.34	...	1	0.05	...	1	
Ce II	-0.17	0.14	3	-0.09	0.06	2	-0.30	0.24	3	-0.52	0.09	2	
Nd II	-0.18	0.20	5	0.37	...	1	0.03	0.13	2	≤ 0.05	...	1	-0.18	0.04	2	-0.06	0.08	3	-0.26	0.17	4	
Eu II	0.31	0.28	2	≤ 0.77	...	1	0.39	0.11	2	0.04	0.20	2	0.21	0.11	2	0.30	0.16	2	
Dy II	0.37	...	1	

^aStar IDs from online version of Stetson (2005).

^bDispersion about the mean abundance.

^cNumber of detected lines.

^dSynthesis of CH band near 4300 Å.

^eUpper limit for 5711 Å Mg I line treated as a detection.

^fIncludes a +0.6 dex non-LTE correction for the 3961 Å line.

^g[Fe/H] from Fe I lines. All [X/Fe] refer to [Fe/H] from Fe I. The same solar abundances as are used as in Table 7.

Table 7. Abundances for Red Giant Members of NGC 7099

ID ^a Species	Stet [X/Fe] (dex)	31 Log[$\epsilon(X)$] (dex)	N ^b	σ^c (dex)	Stet Log[$\epsilon(X)$] (dex)	34 N ^b	σ^c (dex)	AL Log[$\epsilon(X)$] (dex)	38 N ^b	σ^c (dex)	Stet Log[$\epsilon(X)$] (dex)	42 N ^b	σ^c (dex)	Stet Log[$\epsilon(X)$] (dex)	81 N ^b	σ^c (dex)
C ^d	-0.11	6.09	1	...	5.76	1	...	5.48	1	...	6.36	1	...	5.73	1	...
O I	0.76	7.20	3	0.08	6.86	2	0.21	6.91	3	0.17	7.26	3	0.13	6.65	1	...
Na I	0.20	4.13	4	0.10	4.18	4	0.09	4.33	4	0.14	3.89	2	0.11	4.49	4	0.22
Mg I	0.53	5.68	7	0.17	5.82	7	0.12	5.53	7	0.08	5.57	7	0.20	5.41	7	0.17
Al I ^e	0.21	4.29	1	...	4.75	1	...	4.82	1	...	4.07	1	...	4.85	2	0.11
Si I	0.46	5.62	8	0.11	5.69	9	0.10	5.64	9	0.10	5.62	4	0.18	5.69	6	0.12
K I	0.57	3.30	1	...	3.48	1	...	3.19	1	...	3.15	1	...	3.39	1	...
Ca I	0.28	4.25	21	0.16	4.31	23	0.15	4.15	21	0.15	4.24	20	0.18	4.20	20	0.14
Sc II	0.23	0.94	10	0.10	0.91	10	0.11	0.88	10	0.08	0.89	7	0.14	0.87	8	0.13
Ti I	0.21	2.81	22	0.10	2.84	18	0.06	2.68	18	0.09	2.76	17	0.09	2.79	17	0.05
Ti II	0.41	3.01	22	0.13	2.97	20	0.14	2.97	20	0.15	2.99	21	0.13	2.87	24	0.15
V I	-0.22	1.39	1	...	1.59	3	0.06	1.20	1	...	1.27	1	...	1.28	1	...
Cr I	-0.32	2.96	9	0.09	3.07	10	0.11	2.88	10	0.13	2.95	10	0.08	2.88	10	0.12
Mn I	-0.39	2.61	6	0.06	2.57	7	0.05	2.59	7	0.08	2.56	6	0.13	2.50	6	0.13
Fe I ^f	-2.39	5.06	121	0.13	5.13	125	0.14	4.97	115	0.14	4.99	99	0.15	4.97	107	0.13
Fe II	0.05	5.11	16	0.14	5.11	20	0.11	5.09	20	0.13	5.05	15	0.19	5.01	16	0.14
Co I	-0.26	2.27	1	...	2.29	2	0.05	2.33	2	0.16	2.39	1	...	2.42	1	...
Ni I	0.02	3.88	14	0.18	3.87	16	0.18	3.77	16	0.16	3.86	9	0.23	3.86	6	0.19
Cu I	-0.77	1.05	1	...	1.12	1	...	1.01	1
Zn I	0.14	2.35	2	0.11	2.33	2	0.05	2.29	2	0.01	2.33	2	0.05	2.37	2	0.17
Sr II	0.01	0.52	2	0.14	0.45	2	0.16	0.52	2	0.06	0.52	2	0.12	0.48	2	0.05
Y II	-0.10	-0.25	6	0.08	-0.41	6	0.02	-0.50	6	0.15	-0.26	6	0.15	-0.32	5	0.12
Zr II	0.33	0.54	3	0.13	0.49	3	0.15	0.44	3	0.16	0.66	3	0.18	0.47	3	0.08
Ba II	-0.10	-0.35	4	0.08	-0.44	4	0.07	-0.41	4	0.07	-0.44	4	0.12	-0.45	4	0.06
La II	-0.15	-1.40	4	0.22	-1.26	5	0.08	-1.37	5	0.05	-1.07	4	0.13	-1.20	4	0.13
Ce II	0.11	-0.73	4	0.23	-0.92	5	0.16	-1.04	4	0.11	-0.71	1	...	-0.45	1	...
Nd II	0.25	-0.64	7	0.14	-0.81	10	0.10	-0.77	10	0.08	-0.63	4	0.18	-0.83	2	0.09
Sm II	-1.30	2	0.02
Eu II	0.40	-1.48	2	0.04	-1.72	4	0.20	-1.45	3	0.05	-1.38	2	0.04	-1.51	2	0.01
Dy II	0.64	-0.65	1	...	-0.68	2	0.27	-0.98	2	0.30	-0.71	1	...	-1.13	1	...

^aStar IDs from online version of Stetson (2005) or from Alcaino & Liller (1980).

^bNumber of detected lines.

^cDispersion about the mean abundance.

^dSynthesis of CH band near 4300 Å.

^eIncludes a +0.6 dex non-LTE correction for the 3961 Å line. Including this correction, the very marginal detections of the 6696 Å line give consistent Al abundances.

^f[Fe/H] from Fe I lines. All [X/Fe] refer to [Fe/H] from Fe I.

Table 8a. Abundance Sensitivities – Absolute Abundances [X/H]

Species	T_{eff} (+250 K) ^a	$\log(g)$ (−0.5 dex) ^b	[Fe/H](model) (−0.5 dex)	v_t (+0.2 km s ^{−1})
	(dex)	(dex)	(dex)	(dex)
C(CH) ^c	0.28	0.15	−0.13	−0.07
O I ^d	0.04	−0.21	−0.13	−0.01
Na I	0.57	0.22	0.06	−0.10
Mg I	0.23	0.16	0.18	−0.08
Al I	0.34	0.20	0.14	−0.04
K I	0.42	0.05	0.13	−0.07
Ca I	0.28	0.09	0.12	−0.04
Sc II	0.00	−0.16	−0.08	−0.03
Ti I	0.63	0.08	0.21	−0.05
Ti II	−0.03	−0.04	0.01	−0.10
V I	0.54	0.06	0.14	0.00
Cr I	0.55	0.12	0.23	−0.08
Mn I	0.42	0.11	0.17	−0.04
Fe I	0.42	0.06	0.13	−0.07
Fe II	−0.17	−0.08	0.00	−0.09
Co I	0.45	0.05	0.11	−0.01
Ni I	0.42	0.02	0.09	−0.02
Cu I	0.44	0.06	0.12	−0.01
Sr I	0.44	0.12	0.17	0.00
Sr II	0.10	0.04	−0.02	−0.07
Y II	0.02	−0.11	−0.03	−0.03
Ba II	0.13	−0.16	−0.08	−0.14
La II	0.09	−0.14	−0.06	−0.02
Ce II	0.07	−0.10	−0.03	−0.02
Nd II	0.10	−0.14	−0.07	−0.02
Eu II	0.06	−0.08	−0.02	−0.09

^a T_{eff} changes from 4250 to 4500 K.

^b $\log(g)$ changes from 1.0 to 0.5 dex.

^cThe 4320 Å region of the G band of CH was used.

^dValues for the [O I] lines 6300, 6363 Å.

Table 8b. Abundance Ratio Sensitivities

Species	rms Total ^a (dex)	ΔT_{eff} (100 K) (dex)	$\Delta \log(g)$ (0.1 dex) ^b (dex)	$\Delta [\text{Fe}/\text{H}]$ (model) (0.1 dex) (dex)	Δv_t (+0.2 km s ⁻¹) (dex)	W_{λ} ^b (dex)
C(CH) ^c	0.11	−0.06	0.02	−0.05	0.00	0.08
[O I/Fe I] ^d	0.13	0.08	−0.03	−0.05	−0.01	0.08
[Na I/Fe I]	0.15	0.06	0.03	−0.03	−0.10	0.08
[Mg I/Fe I]	0.12	−0.08	0.02	0.02	−0.08	0.05
[Al I/Fe I]	0.08	−0.03	0.03	0.00	−0.04	0.06
[K I/Fe I]	0.11	0.00	0.00	0.00	−0.07	0.08
[Ca I/Fe I]	0.07	−0.06	0.01	0.00	−0.04	0.02
[Sc II/Fe II]	0.09	0.07	−0.02	−0.03	−0.03	0.03
[Ti I/Fe I]	0.11	0.08	0.00	0.03	−0.05	0.02
[Ti II/Fe II]	0.12	0.06	0.01	0.00	−0.10	0.03
[V I/Fe I]	0.07	0.05	0.00	0.00	0.00	0.05
[Cr I/Fe I]	0.11	0.05	0.01	0.04	−0.08	0.03
[Mn I/Fe I]	0.06	0.00	0.01	0.02	−0.04	0.03
[Fe I/Fe I]	0.07	0.00	0.00	0.00	−0.07	0.01
[Fe II/Fe I]	0.26	−0.24	−0.03	−0.05	−0.09	0.03
[Fe II/Fe II]	0.09	0.00	0.00	0.00	−0.09	0.03
[Co I/Fe I]	0.08	0.01	0.00	−0.01	−0.01	0.08
[Ni I/Fe I]	0.04	0.00	−0.01	−0.02	−0.02	0.02
[Cu I/Fe I]	0.08	0.01	0.00	0.00	−0.01	0.08
[Sr I/Fe I]	0.08	0.01	0.01	0.02	0.00	0.08
[Sr II/Fe II]	0.15	0.11	0.02	−0.01	−0.07	0.08
[Y II/Fe II]	0.09	0.08	−0.01	−0.01	−0.03	0.04
[Ba II/Fe II]	0.19	0.12	−0.02	−0.03	−0.14	0.05
[La II/Fe II]	0.14	0.10	−0.01	−0.02	−0.02	0.08
[Ce II/Fe II]	0.11	0.10	0.00	−0.01	−0.02	0.06
[Nd II/Fe II]	0.13	0.11	−0.01	−0.03	−0.02	0.06
[Eu II/Fe II]	0.14	0.09	0.00	−0.01	−0.09	0.06

^aThe rms sum of all 5 contributing terms, relative to whichever of Fe I or Fe II gave the smaller value.

^bAssumed to be 0.08 dex/ $\sqrt{N(\text{lines})}$.

^cThe 4320 Å region of the G band of CH was used.

^dValues for the [O I] lines 6300, 6363 Å.

Table 9. Mean Abundances for Red Giant Members of NGC 2419 and of NGC 7099

Species	NGC		N. Stars	NGC		N. Stars
	$\langle [X/Fe] \rangle^a$	$\sigma[X/Fe]$		$\langle [X/Fe] \rangle^a$	$\sigma[X/Fe]$	
$\log[\epsilon(\text{Fe})](\text{FeI})$	-2.42	0.07	5	-2.06	0.10	7
$\log[\epsilon(\text{Fe})](\text{FeII})$	-2.38	0.04	5	-2.12	0.07	7
[C/Fe]	-0.28	0.35	5	-0.70	0.25	5
[O/Fe]	0.35	0.28	5	0.74	0.10	2
[Na/Fe]	0.29	0.27	5	0.09	0.31	7
[Mg/Fe]	0.51	0.11	5	0.30	0.36	7
[Al/Fe] ^b	0.51	0.36	5	0.45	...	1
[Si/Fe]	0.52	0.07	5	0.43	0.12	5
[K/Fe]	0.61	0.10	5	0.58	0.28	6
[Ca/Fe]	0.29	0.05	5	0.15	0.07	7
[ScII/FeII]	0.18	0.03	5	0.17	0.14	7
[Ti/Fe]	0.21	0.05	5	0.11	0.07	7
[TiIII/FeII]	0.35	0.03	5	0.30	0.16	7
[V/Fe]	-0.23	0.09	5	0.03	0.09	7
[Cr/Fe]	-0.30	0.03	5	-0.23	0.09	7
[Mn/Fe]	-0.40	0.06	5	-0.28	0.07	7
[FeII/FeI]	0.05	0.05	5	-0.06	0.05	7
[Co/Fe]	-0.16	0.12	5	0.09	0.08	4
[Ni/Fe]	0.02	0.07	5	-0.05	0.03	7
[Cu/Fe]	-0.76	0.17	3	-0.61	0.10	7
[Zn/Fe]	0.16	0.07	5	-0.20	0.06	4
[Sr/Fe]	-0.23	0.13	4
[SrII/FeII]	-0.03	0.05	5	-0.08	0.12	3
[YII/FeII]	-0.23	0.15	5	-0.36	0.09	7
[BaII/FeII]	-0.18	0.04	5	-0.11	0.14	7
[LaII/FeII]	-0.02	0.17	5	0.05	0.30	4
[NdII/FeII]	0.14	0.10	5	0.00	0.23	6
[EuII/FeII]	0.41	0.18	5	0.30	0.15	5

^a[X/Fe] where both species are neutral, unless otherwise indicated.

^bA non-LTE correction of +0.6 dex has been applied to abundances derived from the 3961 Å line of Al I.

Table 10. Comparison of Our Mean Abundances for Red Giant Members of NGC 7099
With Those From the Carretta et al VLT Large Program

Species	Carretta et al ^{ab} (dex) (Mean, σ)	This Paper ^c (dex) (Mean, σ)	Notes
[Fe/H]	−2.35 (0.05)	−2.42 (0.07)	
[O/Fe]	0.46 (0.20)	0.35 (0.28)	d, e
[Na/Fe]	0.35 (0.25)	0.29 (0.27)	d
[Mg/Fe]	0.51 (0.04)	0.51 (0.11)	
[Al/Fe]	0.77 (0.32)	0.51 (0.36)	d, e
[Si/Fe]	0.34 (0.07)	0.52 (0.07)	
[Ca/Fe]	0.31 (0.03)	0.29 (0.05)	
[Ba/Fe]	−0.18 (0.04)	−0.22 (0.14)	f, g

^aCarretta et al 2009abc, Carretta et al 2010.

^bUVES sample of 10 RGB stars in NGC 7099.

^cOur sample of 5 RGB stars.

^dThis element has a large internal abundance range.

^eThere are many upper limits in the VLT sample, which E. Carretta (private communication) advises they treated as detections to calculate their mean abundance ratios.

^fFrom the large intermediate resolution FLAMES/VLT survey, see D’Orazi et al (2010).

^gThis, for our result, is the ratio [Ba II/Fe II].

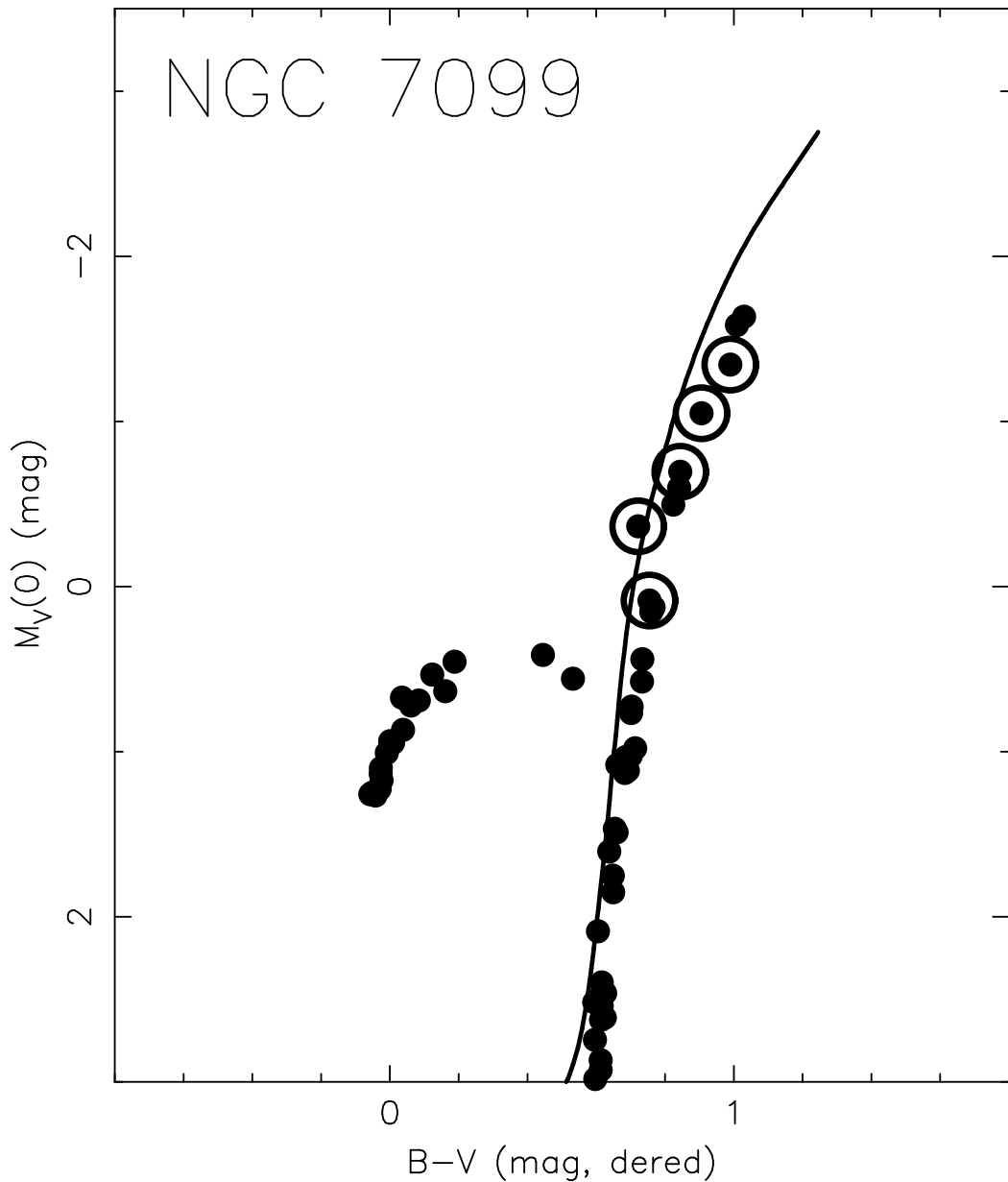


Fig. 1.— A $M_V(0) - (B - V)_0$ CMD for NGC 7099 is shown from the Stetson (2005) on-line database. The RGB stars in our HIRES sample are circled. This is a sparse cluster, and there are few stars on the upper RGB. An α -enhanced Y2 isochrone (Yi et al. 2003) with [Fe/H] = -2.2 dex and age of 12 Gyr is shown.

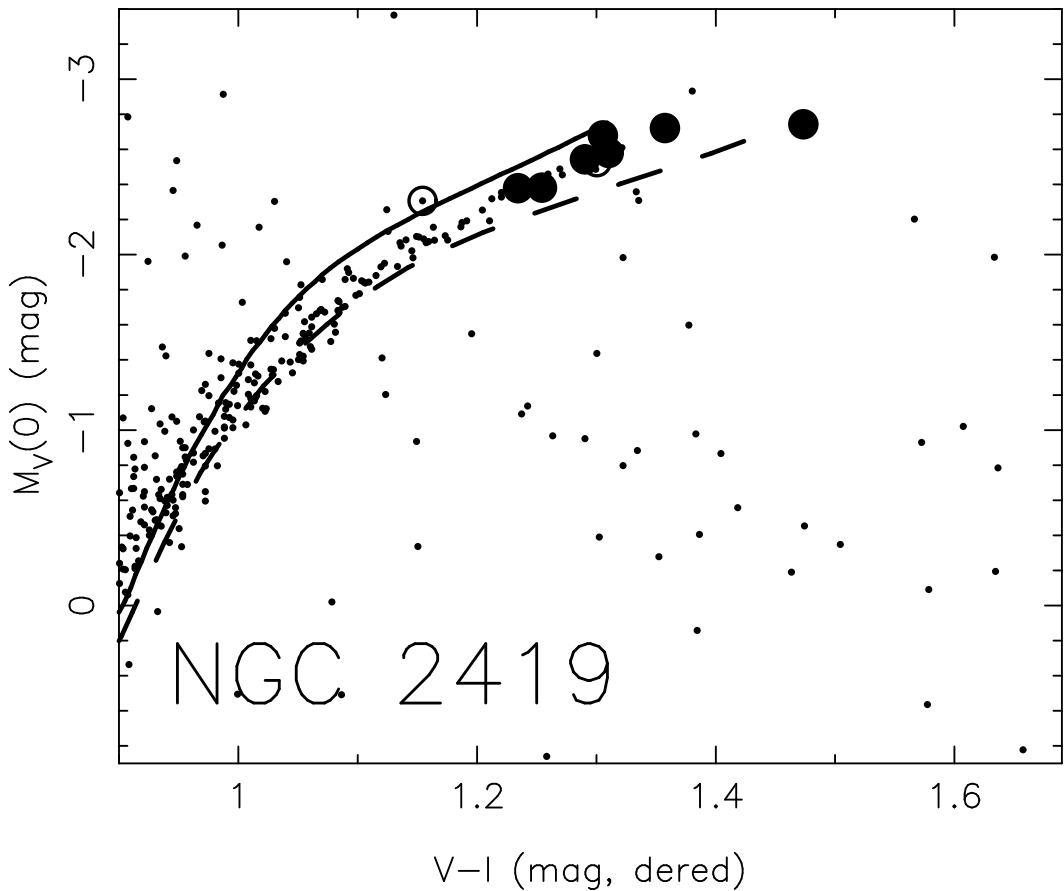


Fig. 2.— A $M_V(0) - (V - I)_0$ CMD for the RGB in NGC 2419 is shown from the Stetson (2005) on-line database. The 7 giants in our HIRES sample are indicated by large filled circles. Two other stars with lower SNR HIRES spectra, whose membership is questionable, are indicated by open circles. The two 12 Gyr Y2 isochrones (Yi et al. 2003) shown have $[Fe/H] = -2.2$ and -1.9 dex, with $[\alpha/Fe] = +0.3$ dex.

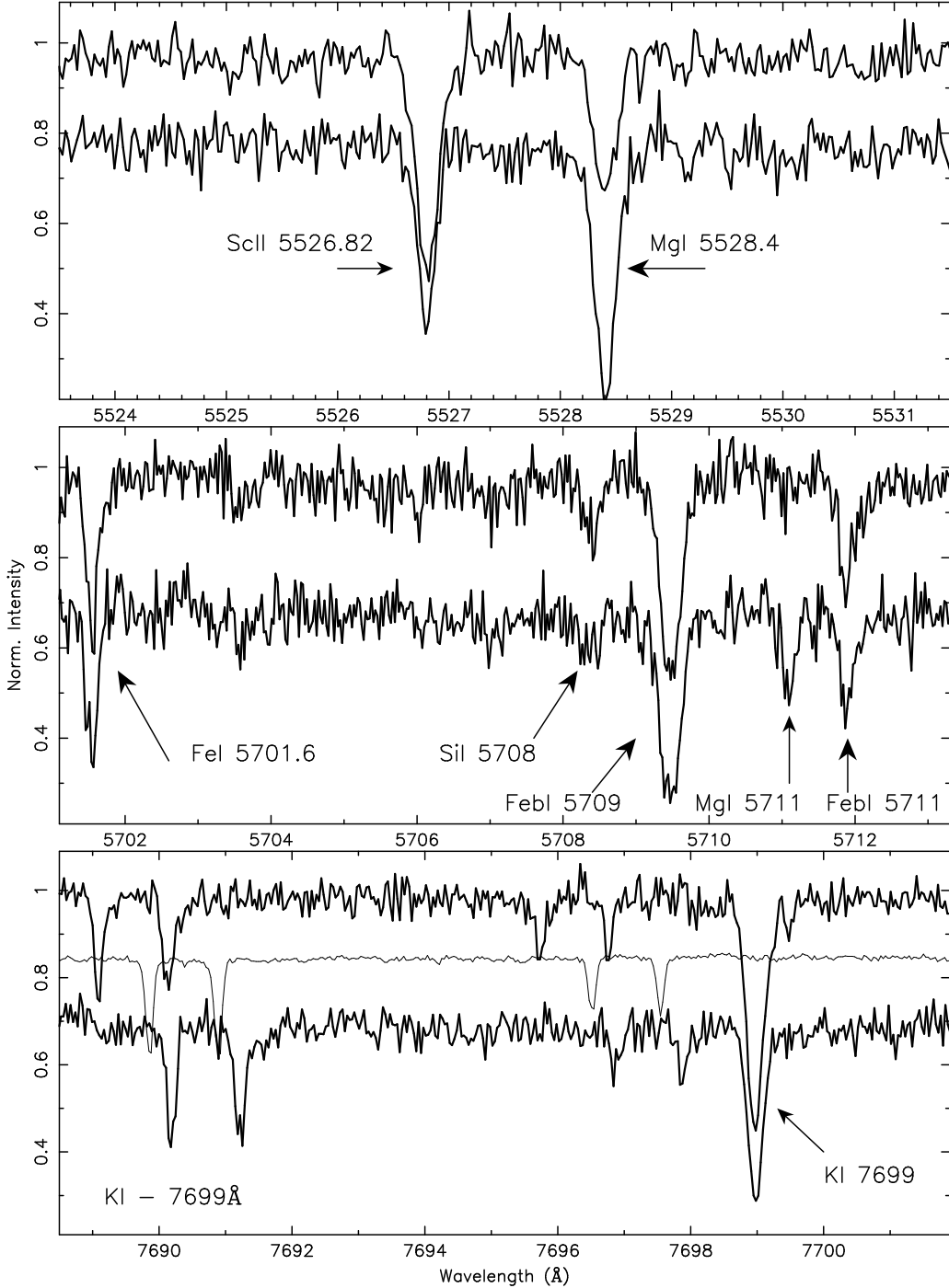


Fig. 3.— The regions of the spectrum near two Mg I lines and a line of K I, shifted in wavelength into the rest frame, are shown for NGC 2419 S1131 as compared to S1209, whose spectrum is shifted slightly lower for clarity. These two giants differ in V by 0.2 mag and in deduced T_{eff} by less than 100 K. The lines identified include a number of blends of FeI lines or FeI and NiI lines labeled as “Febl”. S1131 is more metal-rich and Mg-poor than S1209 and the other NGC 2419 giants. The thin line in the bottom panel is that of a rapidly rotating B star. The slight shifts in wavelength of the telluric lines between the spectra is a reflection of the differing heliocentric corrections for each spectrum.

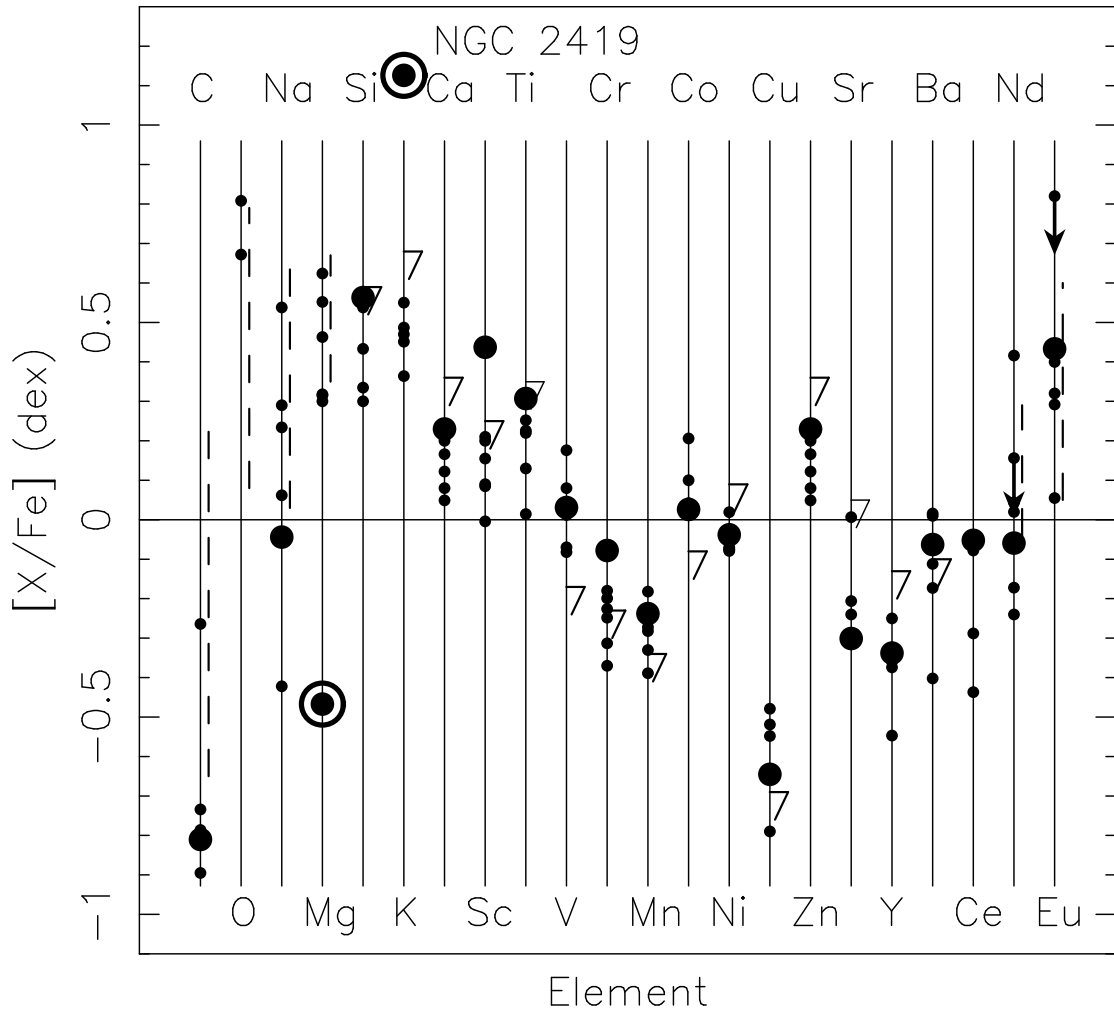


Fig. 4.— Abundance ratios for the detected elements in the NGC 2419 sample of 7 red giants, with the large filled circles indicating S1131. The highly unusual abundance ratios of $[{\rm Mg}/{\rm Fe}]$ and $[{\rm K}/{\rm Fe}]$ for NGC 2419 S1131 are circled. The reference species is FeI for neutral species and FeII for ionized ones. The averages of TiI and TiII and of SrI and SrII are plotted when both are available. Average abundance ratios from our analyses of HIRESr spectra of red giants in the inner halo cluster M30 (NGC 7099) are indicated by “7”. For elements with a large range in M30, the range is indicated by a dashed line.

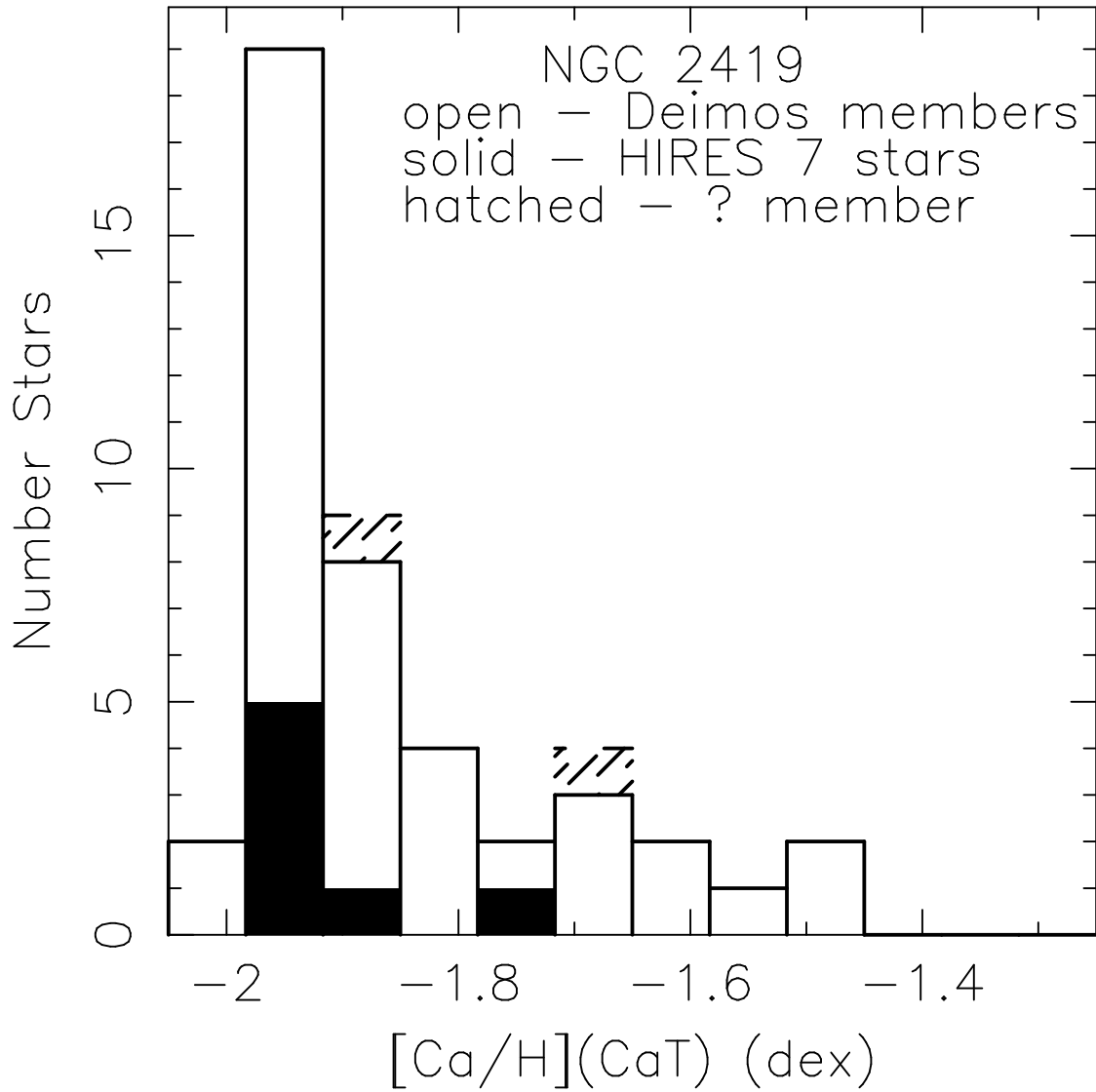


Fig. 5.— A histogram of [Ca/H] as inferred from the Deimos moderate resolution spectra of Cohen et al. (2010) is shown for the sample of 43 definite members of NGC 2419 isolated in that paper. The present sample of 7 RGB stars in this GC with HIRES spectra is shown by the solid fill. The two additional stars in the Deimos survey which are probable members, both of which have low SNR HIRES spectra, are indicated by the hatched areas, which are placed above the histogram defined by the definite members.